DECLARATION

I declare that the work submitted is the result of my investigation and is not submitted in candidature for any other degree.

Mr. G.K. Chinyama
Candidate

Prof. C.V. Sheth
Chairman,
Board of Examiners
of M.Sc. Thesis.

Dr. M. Chirwa
Acting Head,
Physics Dept..

A STUDY OF THE ELECTRONIC AND THERMAL STRAINS IN DIRECT AND INDIRECT BAND-GAP SEMICONDUCTORS BY THE USE OF PHOTOACOUSTIC SPECTROSCOPY

A PHYSICS RESEARCH PROJECT REPORT SUBMITTED TO THE

PHYSICS DEPARTMENT

IN THE SCHOOL OF NATURAL SCIENCES

AT THE

UNIVERSITY OF ZAMBIA

IN PARTIAL FULFILLMENT OF THE REQUIREMENTS FOR THE

AWARD OF THE DEGREE OF

MASTER OF SCIENCE (M.Sc.) IN PHYSICS

BY

GODFREY KAUMBA CHINYAMA

OCTOBER, 1989.

DEDICATION

Congratulations my father, Chinyama Lizu, and my sister, Sombo, for the combined effort that you two have put in to see me to this level.

God Shall Bless You!

CONTENTS

Page

Acknowledgement:............................(iii)

Abstract:....................................(v)

CHAPTER 1: INTRODUCTION 1

1.1. PREVIEW:....................................1

1.2. BASIC IDEAS:................................5

1.3. THE PROCESS OF THERMAL DIFFUSION:..........11

1.4. DERIVATION OF THE ACOUSTIC GENERATION:.....15

1.5. DETERMINATION OF THE ELECTRONIC AND
THERMAL STRAINS:............................18

1.6. OBJECTIVE OF THIS WORK:....................20

CHAPTER 2: A REVIEW OF THE APPARATUS 24

2.1. ACOUSTO-OPTIC MODULATION:..................24

2.2. PIEZOELECTRIC DETECTION:...................33

2.3. PHASE SENSITIVE DETECTION:.................42

CHAPTER 3: THE EXPERIMENTAL WORK 53

3.1. CALIBRATION OF THE APPARATUS:..............53

3.1.1. Calibration of the Phase
Sensitive Detection System.........53

3.1.2. Calibration of the Piezoelectric Transducer.........................59

3.1.3. Calibration of the Semiconductor...65

3.2. SAMPLES AND MATERIALS:.....................74

3.3. EXPERIMENTAL PROCEDURE:...................79

CHAPTER 4: RESULTS 85

4.1. VERIFICATION OF THE PHASE RELATIONSHIPS BETWEEN THE ELECTRONIC AND THERMAL PHOTOACOUSTIC SIGNALS:........85

4.2. CALCULATION OF THE ELECTRONIC AND THERMAL PHOTOACOUSTIC SIGNALS:............97

CHAPTER 5: DISCUSSION AND CONCLUSION 99

5.1. DISCUSSION:..............................99

5.2. CONCLUSION:.............................101

REFERENCES:................................104

ACKNOWLEDGEMENTS

It has been possible to produce this research project report due to the influence of many people who have made contributions to me, in one way or the other. Although it is not possible to list here the names of all those I am indebted to in this regard, I want them to know that I really deeply appreciate their help.

Particular thanks must be given to the British Government through the British Council for providing the financial support to enable me to go and conduct this research work at the University of Surrey, in the United Kingdom. Without this support, it would not have been easy for me to finish in the shortest time possible. I am also grateful to the Physics Department, University of Surrey for providing the facilities and staff which made it possible for me to conduct this research work on their Campus. Infact special thanks must go to Dr. K.W.H. Foulds, my project Supervisor, whose guidance throughout the course of the work will remain a valuable lesson in any of my future research work. I really enjoyed his company, and through him, I learned a lot of research skills.

I have great pleasure in thanking the University of Zambia, especially the Physics Department, for the all round support it has rendered to me in all the phases of this postgraduate course programme. Special acknowledgements must be extended to Prof. C.V. Sheth, for his supervision in making sure that I finished this work in time, and Dr. M. Chirwa for suggesting the necessary changes to the report. Their help has been instrumental in putting the final version together.

Last, but not the least, I wish to thank Mr. Godfrey Shevwanti for succeeding in turning my scrawls into excellent drawings.

I extend my grateful thanks to all these people. Any merit which this volume may possess, is without doubt , due to their efforts; the defects are probably my fault.

G.K.C.

Lusaka, Oct. 1989.

ABSTRACT

When a modulated beam of light impinges on a solid, elastic waves are produced as a result of the surface motion due to thermal expansion. In semiconductors, in addition to this thermal expansion effect, there is also mechanical strain induced in the material due to the photogeneration of excess free carriers. Theory predicts the dependence of this strain on the pressure dependence of the energy gap, dE_g/dp, thereby giving a theoretical foundation for the study of the difference of this effect in a direct band_gap semiconductor and an indirect band_gap semiconductor in view of the difference in sign of their pressure coefficients of the band gap.

An experiment has been performed to investigate this difference by carrying out photoacoustic measurements on the magnitude and phase of the acoustic signals generated as a result of these effects, in GaAs (direct) and silicon (indirect). In GaAs, the results have been found to be very unsatisfactory due to the experimental factors cited. As for silicon, no results have been obtained because it required

modulation frequencies of over 1MHz in order to sustain a detectable strain. However from the information obtained, we learn that the electronic strain is the dominant contributor to the total acoustic signal, in both cases. Measures to take in order to improve the situation have been explored in some detail. The importance of the beam spot size has been highlighted. Generally, several important points which need more attention have been revealed.

CHAPTER ONE

INTRODUCTION

1.1 PREVIEW

Photoacoustic microscopy has emerged as a useful technique to investigate optical and thermal properties at and near the surface of a material[1,2,3,4]. This technique although new is an outgrowth of a much older method most commonly refered to as Photoacoustic Spectroscopy(PAS). The photoacoustic effect, in which optical energy absorbed by a sample is detected through the subsequent thermal generation of acoustic signals was discoverd by Alexander Graham Bell more than 100 years ago[5]. Only recently has it developed into a popular research and analytical tool in such areas as Physics, Chemistry, Biology and Medicine.

PAS of solids typically involves the irradiation of a surface of an usually opaque sample with an intensity modulated optical(laser) or electron beam focussed and scanned across the surface. Localised periodic heating results from the absorption of the incident beam. The solution to the periodic thermal diffusion equation appropriate to this situation is a 'thermal wave' very highly damped so that it propagates not more than a wavelength. Infact this wave is attenuated to 1/e after propagating one reduced wavelength

$$\mu = \lambda/2 \tag{1.1}$$

where λ is the wavelength and μ is referred to as the 'thermal diffusion length' given by

$$\mu = \left(\frac{2k}{\omega c \rho}\right)^{1/2} \tag{1.2}$$

Here k is the thermal conductivity, ρ the density, c the specific heat capacity, and ω the frequency at which the heat is being produced. In spite of their being damped, thermal wave interactions with sample features may be treated mathematically as scattering and reflection interactions, just as is the case with the conventional optical and acoustic waves.

The thermal waves generated in the sample by the absorption of the optical (photon or electron) beam will, through their various interactions, provide thermal wave images of those surface and subsurface features with different thermal characteristics. As in optics and acoustics, the resolution achieved in thermal wave imaging is set both by the spot size of the optical or electron beam and by the reduced wavelength of the thermal waves. This wavelength, as may be seen from equation (1.2) is in turn determined by the frequency at which the optical beam is modulated. Thermal waves are most difficult to detect directly since, because of their strong damping, they will only penetrate 10 m in silicon at 200KHz - 20MHz. However associated with these thermal waves are acoustic waves of the same frequency but of much longer wavelengths (5cm - 0.5mm). These acoustic waves have a very large range and can be readily detected with a piezoelectric transducer in contact with the sample, as applied in most photoacoustic experiments. However, because of their large wavelengths, the acoustic waves at these frequencies do not interact with or image any of the microscopic features in the sample but serve simply as the carriers of the imaging information generated by the much shorter thermal waves.

Up to now, thermal_wave imaging and microscopy have been used primarily for the detection and imaging of subsurface features in opaque samples[6,7,8,9]. At low frequencies, where the thermal wavelengths are large, the subsurface features are macroscopic in size. Rosencwaig and Bussel[8] and Brandis and Rosencwaig[10] have demostrated thermal_wave imaging of microscopic subsurface features at 100KHz or more, using laser scanning and electron beam scanning, respectively.

Thermal_wave microscopy can, however, be used for more than subsurface imaging, in particular to image surface thermal features which are otherwise invisible to either optical or electron probes. The thermal features so imaged are those areas in the sample with sufficiently different thermal characteristics from their surroundings so as to cause scattering and changes in propagation of the thermal waves when they enter these regions. It has already been demostrated that changes in a sample's thermal properties due to structural phase changes or changes in crystallinity can be readily detected with a thermal wave or a photoacoustic technique.

However, one of the most promising application of the technique appears to be in the study of semiconductor devices. For example thermal_wave electron microscopy has been used at 640KHz modulation frequency to detect and image p_doped silicon regions in a bare silicon wafer[13]. In such work, it has generally been assumed that photoacoustic generation in semiconductors is predominantly due to thermoelastic effects. In this report, another important mechanism for photoacoustic generation in semiconductors, that of periodic mechanical stress_strain flunctuations induced through the photogeneration of free carriers, is investigated.

The advantage of this photoacoustic spectroscopy is that the photoacoustic signal is directly related to the amount of strain induced in the material, due to both the generation of electrons and holes and the thermal heating. Changes in material or geometric structure will change the absorption or reflection charateristics at the absorbing surface and alter the photoacoustic signal, thus visual information about the local thermal and elastic properties on a microscopic scale is provided. Information about de_excitation processes, also on a microscopic scale is obtained. This technique shows an excellent way for non_destructive investigation of bulk materials. Besides, photoacoustic methods use inexpensive lasers and simple electronics to produce the image in not less than a few minutes. This is an advantage because the sample should not be heated for a long time as this may cause distortions in the 'image_forming' thermal waves.

1.2. BASIC IDEAS

From the band model for the diamond type crystals (i.e. crystals with cubic symmetry), the band

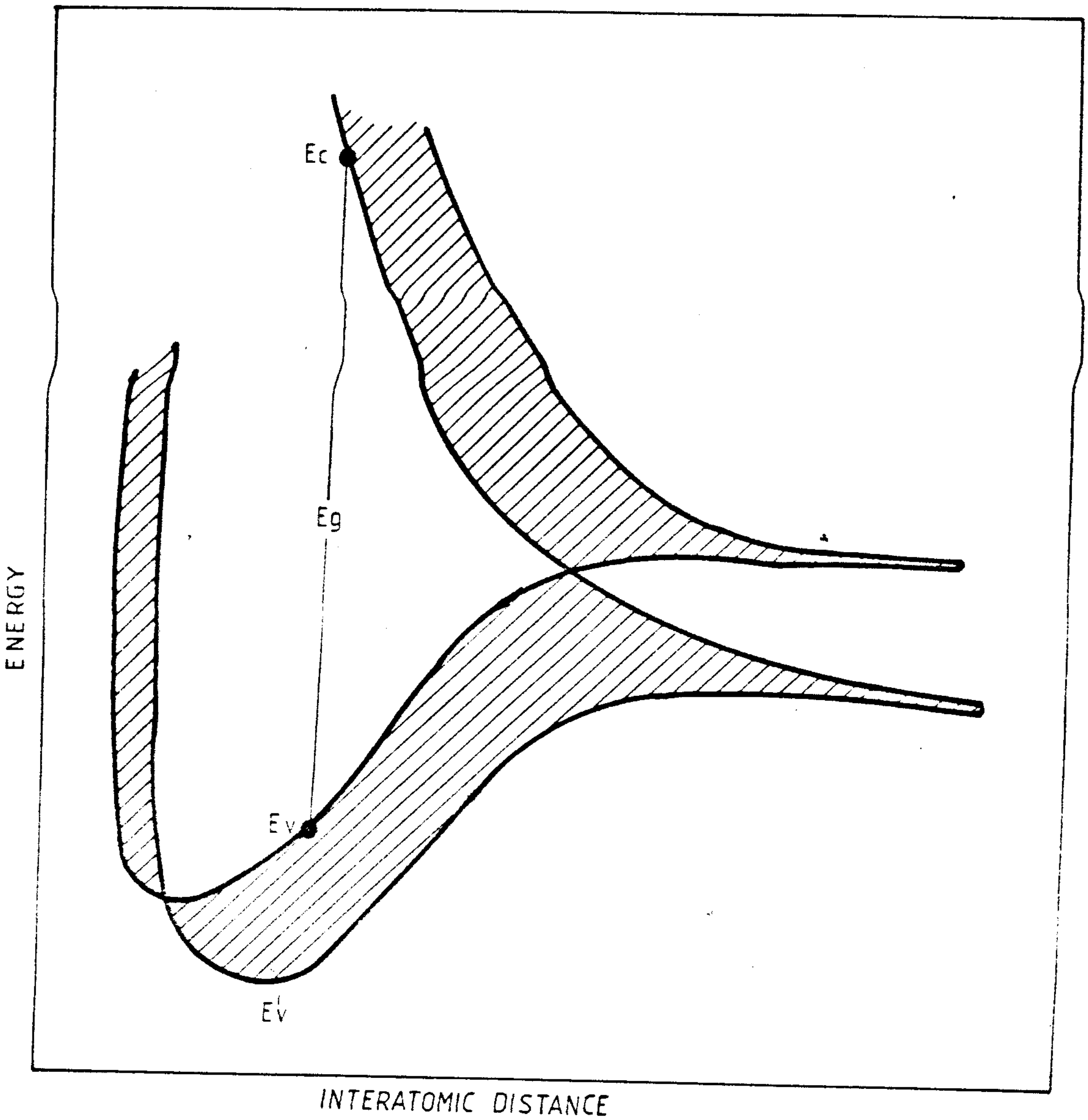

Fig. 1. Band Structure of the Diamond Type Crystals

structure versus interatomic distance is found as shown schematically in Figure 1[14]. The bottom of the conduction band corresponds to <100> minimum in K_space, while the top of the valence band to <100> minimum, in silicon, for instance. We will consider the intrinsic case for the sake of simplicity but the result is practically the same for the extrinsic case too.

The total energy of the electrons in the conduction and valence bands in the volume unit is

$$E_{tot} = \int_{E_V'}^{E_V} E\, f_n(E,n)\, N_V(E)\, dE + \int_{E_C}^{E_C'} E\, f_n(E,n)\, N_C(E)\, dE \qquad (1.3)$$

E denotes energy, f_n is the electron distribution function, N_c , N_V , are the densities of states in the conduction and valence band,respectively, E_V' , E_V are the energies corresponding to the bottom and to the top of the valence band and E_c, E_c' are the energies corresponding to the bottom and the top of the conduction band.

Introducing into equation (1.3) the distribution function of the holes f_p

$$f_p = 1 - f_n \qquad (1.4)$$

one obtains the relation

$$E_{tot} = \int_{E'_v}^{E_v} E\, N_v\, dE - \int_{E'_v}^{E_v} E\, f_p\, N_v\, dE + \int_{E_c}^{E'_c} E\, f_n\, N_c\, dE \qquad (1.5)$$

The first term in equation (1.5) represents the total energy of electrons in the valence band, W, when the latter is filled up. The two latter terms, for non_degenerate carrier gas, are equal to

$$\left.\begin{aligned} \int_{E'_v}^{E_v} E\, f_p\, N_v\, dE &= p(E_v - 3/2k_B\, T) \\ \int_{E_c}^{E'_c} E\, f_n\, N_c\, dE &= n(E_c + 3/2k_B\, T) \end{aligned}\right\} \qquad (1.6)$$

n, p denote electron and hole concentrations and $(3/2)k_BT$ is the thermal energy of a current carrier. Further we shall put n=p, then from equations (1.5) and (1.6),we get

$$E_{tot} = W + n(E_c - E_v) + 3k_B\, T\, n$$

or

$$E_{tot} = W + nE_g + 3n\, k_B\, T \qquad (1.7)$$

where $E_g = E_c - E_V$ is the energy gap. We shall call by ε dilation (deformation) of the crystal.

$$\varepsilon = \frac{a - a_0}{a_0} \tag{1.8}$$

where a is the actual lattice constant (i.e.with current carriers in the crystal), a_0 is the lattice constant when there are no current carriers. Since all of the state energies depend explicitly on ε , one can write

$$\frac{dE_{tot}}{d\varepsilon} = \frac{dW}{d\varepsilon} + n \frac{dE_g}{d\varepsilon} \tag{1.9}$$

If one assumes that the elastic properties of solids are related to the valence electrons only, then one can get, from the theory of elasticity[15],

$$\frac{dW}{d\varepsilon} = (3C_{11} + 6C_{12})\,\varepsilon \tag{1.10}$$

where C_{11} , C_{12} are the moduli of elasticity. Hence we can write equation (1.9) in the form

$$\frac{dE_{tot}}{d\varepsilon} = 3(C_{11} + 2C_{12})\varepsilon + \frac{3n}{\beta}\left(\frac{\partial E}{\partial p}\right)_T \tag{1.11}$$

where $(\partial E_g/\partial p)_T$ is the pressure dependence of the energy gap, β is the volume compressibility coefficient.

At equilibrium $\frac{dE_{tot}}{d\mathcal{E}} = 0$, and then

$$\mathcal{E} = \frac{1}{3\beta(C_{11} + 2C_{12})} n \left(\frac{\partial E_g}{\partial p}\right)_T$$

or

$$\mathcal{E} = \frac{1}{3}\left(\frac{\partial E}{\partial p}\right)_T n\, \delta_{ij} \tag{1.12}$$

where $\delta_{ij} = \frac{1}{\beta(C_{11} + 2C_{12})}$ is a tensor quantity.

The formula (1.12) gives the dependence of the dilatation of the crystal on current carrier concentration. If the current carriers are generated by light, one can introduce a photostriction coefficient (the meaning of which is deformation of the crystal related to the unit concentration of the electron_hole pairs,

$$\alpha_p = \frac{\Delta\mathcal{E}}{\Delta n}$$

From equation (1.12), one can obtain the expression for α_p as

$$\alpha_p = \frac{\Delta\mathcal{E}}{\Delta n} = \frac{1}{3\beta(C_{11} + 2C_{12})}\left(\frac{\partial E}{\partial p}\right)_T \tag{1.13}$$

It will be worth noting that the sign of this 'strain' effect is the same as the sign of pressure coefficient of the energy gap. This strain should then be positive (dilatation) for direct band_gap semiconductors (GaAs, GaSb, etc.) and negative (contraction) for indirect band_gap semiconductors (Si,GaP, etc.).This is so because it has been observed experimentally that, when a direct band_gap semiconductor is subjected to pressure, the energy gap increases with increase in pressure, whereas for the indirect case, the energy gap narrows with increase in pressure.

In this work, the samples (which are semiconductor wafers) were half_coated with metallic chromium so that when the optical beam is scanned from one side to the other, we have both the electronic and thermal strains occuring on the uncoated side and the thermal strain on the other. Hence there is need to understand, in some detail, the process of thermal diffusion on both sides of the samples.

1.3.THE PROCESS OF THERMAL DIFFUSION

The diffusion equation describing the periodic heating on the bare semiconductor surface may be stated as

$$K\nabla^2 T - j\omega\rho c\, T = 0 \qquad (1.14)$$

where T is the laser induced periodic temperature in the semiconductor, at angular frequency ω, k is the thermal conductivity, ρ is the density and c is the specific heat capacity of the semiconductor. The solution to such an equation is

$$T(x,t) = Ae^{-(\omega/2D)^{\frac{1}{2}}x}\, e^{j(\omega t - (\omega/2D)^{\frac{1}{2}}x)} \qquad (1.15)$$

from where the thermal diffusion length is deduced as $\mu_{th} = (2D/\omega)^{\frac{1}{2}}$.

The flux of heat at the absorbing surface may be treated as a boundary condition. If P is the power of the incident laser beam and hf is the energy of an incident photon of light, then the number of photons arriving per second on the surface is P/hf. If R_S is the optical reflectivity of the semiconductor surface, then $R_S(P/hf)$ is the number of photons reflected per second and hence the effective number of photons illuminating the surface is $(P/hf)(1-R_S)$. Since $hf-[(3/2)K_B T_o + E_g]$ is the effective energy used in heating the sample, the flux of heat at the absorbing surface may be stated as

$$k \left.\frac{dT}{dx}\right|_{x=0} = (1-R_S)\frac{P}{hf}(hf - E_g - 3k_B T_o)\, e^{-(r^2/a^2)} \tag{1.16}$$

Here E_g is the band_gap energy of the semiconductor, k_B is the Boltzmann's constant, T_o is the ambient temperature and the beam is assumed to be Gaussian distributed with radius a. The rapid relaxation to the band edges of the generated electron_hole pairs gives rise to heating in the semiconductor.

The periodically generated carriers in the semiconductor also obey a diffusion equation, which may be stated as

$$D\nabla^2 N - j\omega N + \frac{N}{\tau} = 0 \tag{1.17}$$

where N is the density of carriers, D is the diffusivity of the semiconductor, τ is the excess carrier lifetime. For the undoped GaAs sample used in this experiment, it was estimated (section 3.3) that $\tau \simeq 80\mu s$. The duration of the light pulse at this frequency is $\simeq 5\ \mu s$, so that the rate at which carriers are being generated is greater than the rate at which they recombine. So, since the experiment is being done in a region where $\omega\tau > 1$

the recombination term may be neglected and equation (1.17) reduces to

$$D \nabla^2 N - j\omega N = 0 \qquad (1.18)$$

Just as in thermal diffusion, the carrier density is found to diffuse into the bulk of the semiconductor as an exponentially damped wave (solution of equation (1.18)) with a diffusion length $\mu_e = (2D/\omega)^{\frac{1}{2}}$. In the case of the silicon sample,it was assumed that the carrier lifetime should be much smaller than that for GaAs, in view of the fact that the indirect transition in silicon cannot be detected in the absorption spectrum because of its larger energy and smaller probability. In this case, therefore, the recombination term in equation (1.17) may not be neglected.

Also, the generated carriers produced by the incident laser beam may be treated as another boundary condition at the free semiconductor surface. If we assume that one photon of light, hf, generates an electron_hole pair (i.e. assuming unit quantum efficiency), then P/hf is the number of electron_hole pairs injected per second and $(P/hf)(1-R_S)$ is the effective number of generated electron_hole pairs. The boundary condition may then be stated as

$$D \left.\frac{dN}{dx}\right|_{x=0} = (1-R_S)\frac{P}{hf}\, e^{-(r^2/a^2)} \qquad (1.19)$$

It is also assumed here that surface recombination is negligible. The distribution of the carriers is considered to assume a Gaussian profile.

On the metallized side (i.e. the Cr coated side) of the samples, since the layer of Cr is treated merely as a source of heating at the surface of the semiconductor and hence there is no generation of electron_hole pairs, the flux of heat on this side is simply given by

$$k \left.\frac{dT}{dx}\right|_{x=0} = (1-R_{Cr})\frac{P}{hf}\, e^{-(r^2/a^2)} \qquad (1.20)$$

where R_{Cr} is the reflectivity of the Cr layer. Thermal diffusion within this layer can be ignored as the thermal diffusion length in Cr at 200KHz is $\simeq 7\,\mu m$, which is far larger than the size of the coating thickness.

1.4. DERIVATION OF THE ACOUSTIC GENERATION

In this derivation of the excitations of the acoustic transducer, the theory of Kino and Stearns is used[20]. We will not go into great detail but a brief background will suffice. We let S^o, σ^o, v^o, and u^o, be the stress, strain, velocity, and particle displacement, respectively, when there is no heat source present, and S', σ', v', and u' be the acoustic fields arising due to thermal excitations. According to this theory, both sets of fields obey the following set of equations

$$\vec{\nabla} . S = -\omega^2 \rho \vec{u} \tag{1.21}$$

$$\nabla . \vec{u} = \vec{\sigma} \tag{1.22}$$

$$j\omega \vec{u} = \vec{v} \tag{1.23}$$

The unexcited fields obey the additional relation

$$S^o = C : \sigma^o \quad \text{or} \quad S^o_i = C_{ij} \sigma_j \tag{1.24}$$

whereas the thermally excited fields obey the equation

$$S'_i = C_{ij}(\sigma'_j - \alpha_i T) \tag{1.25}$$

ρ is the density of the sample material and C or C_{ij} its tensor elastic constant, so that equations (1.24) and (1.25) represent tensor products. It is assumed here that all fields have a periodic time dependence with angular frequency ω and T is the laser induced periodic temperature at frequency, ω. The details behind this theory are beyond the scope of this project, hence we will not go into it, except to mention that α_1, α_2, and α_3 are the principal thermal expansion coefficients associated with the principal axes of the crystal, and $\alpha_4 = \alpha_5 = \alpha_6 = 0$. For cubic symmetry, or an isotropic material, $\alpha_1 = \alpha_2 = \alpha_3 = \alpha$ is the linear coefficient of thermal expansion.

This derivation only assumes thermal strains to be present. In this experiment, we have, in addition, the effects of the electronic strain, so that equation (1.25) needs to be modified, in order to accomodate this electronic strain. This is achieved by simply writing equation (1.25) to be of the form

$$S_{ij} = C_{ijkl}\left(\sigma_{kl} - \alpha T \delta_{kl} - \frac{1}{3}\frac{dE_g}{dp}\Delta n \delta_{ij}\right) \qquad (1.26)$$

It can be seen that this equation has been obtained by simply adding the electronic strain term to equation (1.25), just as the thermal term was added to equation (1.24) to obtain equation (1.25).

The excitation of the piezoelectric transducer by the acoustic waves generated in the semiconductor will then be of the form

$$V = A \int_{\mathcal{V}} \Delta^{o} \left(\alpha T + \frac{1}{3} \frac{dE_g}{dp} \Delta n \right) d^3 x \tag{1.27}$$

V is the voltage output at the transducer, A is a proportionality constant whose precise value is not considered important here and $\Delta^{o} = \sigma_{11}^{o} + \sigma_{22}^{o} + \sigma_{33}^{o}$ is the volume dilation of the sample associated with the acoustic fields due to the transducer, if it were driven externally and without any illumination present. Δ^{o} is the volume dilation associated with the almost plane waves incident on the free semiconductor surfaces at the angle of 30 to the surface normal. The integral is taken over the entire volume $\mathcal{V}$ of the sample and the aluminium buffer rod used in the experiment.

1.5. DETERMINATION OF THE ELECTRONIC AND THERMAL STRAINS

The fields N and T in equation (1.27) extend into the samples only by a few microns. As in Kino and Stearns' work, Δ^{o} may be taken to be constant and equal to $\Delta^{o}\big|_{r,x=0}$. From equations (1.14) and (1.18), we have

$$T = \frac{K}{j\omega\rho c} \nabla^2 T \tag{1.28}$$

and

$$N = \frac{D}{j\omega} \nabla^2 N \tag{1.29}$$

Substituting these two equations into equation (1.27) gives

$$V = \frac{A}{j\omega}\left(\Delta^0\Big|_{r,x=0}\right)\int_v \left(\frac{K\alpha}{\rho c}\nabla^2 T + \frac{D}{3}\frac{dE_g}{dp}\nabla^2 N\right) d^3x \tag{1.30}$$

representing the output of the transducer. Equation (1.30) may be rewritten as

$$V = \frac{A}{j\omega}\left(\Delta^0\Big|_{r,x=0}\right)\int_v \left(\frac{K\alpha}{\rho c}\vec{\nabla}\cdot\vec{\nabla} T + \frac{D}{3}\frac{dE_g}{dp}\vec{\nabla}\cdot\vec{\nabla} N\right) d^3x$$

so that by using Gauss's theorem, we obtain

$$V = \frac{A}{j\omega}\left(\Delta^0\Big|_{r,x=0}\right)\int_v \left(\frac{K\alpha}{\rho c}\vec{\nabla} T + \frac{D}{3}\frac{dE_g}{dp}\vec{\nabla} N\right) . dS \tag{1.31}$$

and applying the boundary conditions of equations (1.16), (1.19), and (1.20), we get for the illumination of the bare semiconductor

$$V_S = \frac{A\pi a^2}{j\omega}(1-R_S)\frac{P}{hf}\left(\Delta^\circ\Big|_{r,x=0}\right)$$

$$\times\left[\frac{\alpha}{\rho c}\left(hf - E_g - 3k_BT + \frac{1}{3}\frac{dE_g}{dp}\right)\right] \qquad (1.32)$$

and for the metallized side of the semiconductor, we find

$$V = \frac{A\pi a^2}{j\omega}(1-R_{G})P\left(\Delta^\circ\Big|_{r,x=0}\right)\left[\frac{\alpha}{\rho c}\right] \qquad (1.33)$$

The bracketed expression in equation (1.32) consists of two terms, one involving α, the other involving (dE_g/dp). These terms correspond to the contributions of the thermal and electronic strains, respectively, to the total photoacoustic signal.

1.6. OBJECTIVE OF THIS WORK

It is well known that introduction of excess free carriers results in the local mechanical straining, consisting in a change of lattice constant (dilatation or contraction) of a semiconductor. In the case of diamond type crystals, there are two reasons for this:

(i). a hole in the valence band decreases the energy of the covalent bonds

(ii). an electron in the conduction band introduces some added component of the bonding and anti_bonding energy.

For the case of photogenerated carriers, where an equal number of excess free electrons and holes is assumed, it has been shown (section 1.12) that the local strain produced in a diamond type semiconductor is of the form

$$S = \frac{1}{3}\left(\frac{\partial E}{\partial p}\right)_T \Delta n\, \delta_{ij} \tag{1.34}$$

The parameter $(\partial E_g / \partial p)_T$ denotes the pressure dependence of the energy gap of the semiconductor at constant temperature, and Δn is the number of generated electron_hole pairs. For silicon, it is found that $S^{el}_{ij} = -9.5 \times 10^{-25} \times \Delta n\, \delta_{ij}$, where Δn is expressed in cm^{-3} . This so called electronic strain may be compared with the thermal strain that arises from heating of the semiconductor,

$$S^{th}_{ij} = \alpha\, \Theta\, \delta_{ij} \tag{1.35}$$

where α is the linear coefficient of thermal expansion and Θ is the temperature flunctuation in the semiconductor.

It is clear from the above equations that the mechanical strains due to photocarrier injection and local heating are very similar in form for semiconductors of cubic symmetry. The strains vary linearly with Δn and θ, respectively, and both are isotropic.

In a photoacoustic measurement, we would therefore expect that as long as the incident photon energy is greater than the band gap (i.e. $h\nu > E_g$), the electronic strain will produce acoustic waves in the semiconductor in a manner analogous to the thermal strain. Furthermore, in the case of indirect band_gap semiconductors (e.g. silicon) where $\alpha = 3 \times 10^{-6}\ {}^{o}C^{-1}$, it is clear that the electronic and thermal strains will be of opposite sign. Hence we would expect acoustic waves generated from photoinjection of free carriers in silicon to be opposite in phase to acoustic waves generated from the periodic heating of the silicon. On the other hand, in direct band_gap semiconductors (e.g. Gallium Asenide), the two strains will be of the same sign and hence we should expect the acoustic signals generated in both cases to be in phase.

The aim of this work was therefore to verify this phenomenon and investigate the importance of the electronic strain in photoacoustic generation in both the direct and indirect band_gap semiconductors. As materials for investigation, silicon (indirect) and Gallium Asenide (direct) were chosen, for convenience reasons.

CHAPTER TWO

A REVIEW OF THE APPARATUS

In this chapter, components which have been used in the photoacoustic detection and measurements reported in this work are reviewed. These include the Acousto_optic modulation technique, the Piezoelectric transducer and the Phase Sensitive Detector (PAS).

2.1. ACOUSTO-OPTIC MODULATION

The study of acousto_optic deflectors/modulators represents a direct application of the laws of diffraction of light by acoustic waves. Acousto_optics deals with interactions between acoustic waves and light so that acousto_optic modulators utilise acousto_optic interaction ultrasonically to vary the amplitude or phase of a light beam. This acousto_optic interaction is a way of influencing the propagation characteristics of an optical beam by applying a low frequency acoustical field to the medium through which the light wave passes.

Acousto_optic devices are based on a deflector or light modulator consisting of a transparent medium in which ultrasound is propagated. The acoustic waves can be progressive or stationary, plane or focussed in the region where they interact with the beam of light. These waves are produced by a piezoelectric transducer, which itself consists of a material which can be a monocrystal, thin layers deposited by evaporation or a ceramic like the ones discussed in section 2.2. In acousto_optic deflectors/modulators a certain proportion of the incident light from a laser source is deflected in one (or more) direction due to periodic variations in the index produced by the passage of the acoustic waves.

Fig.2. represents a typical example of light diffraction by acoustic waves. λ^* is the acoustic wavelength, λ that of light, the interaction length L is the dimension of the acoustic beam in the direction of propagation of light, D is the width of the light beam in the direction of propagation of acoustic waves and in a Bragg diffraction, the angle of incidence θ_B is equal to half the angle of deflection, itself equal to the ratio λ/λ^*.

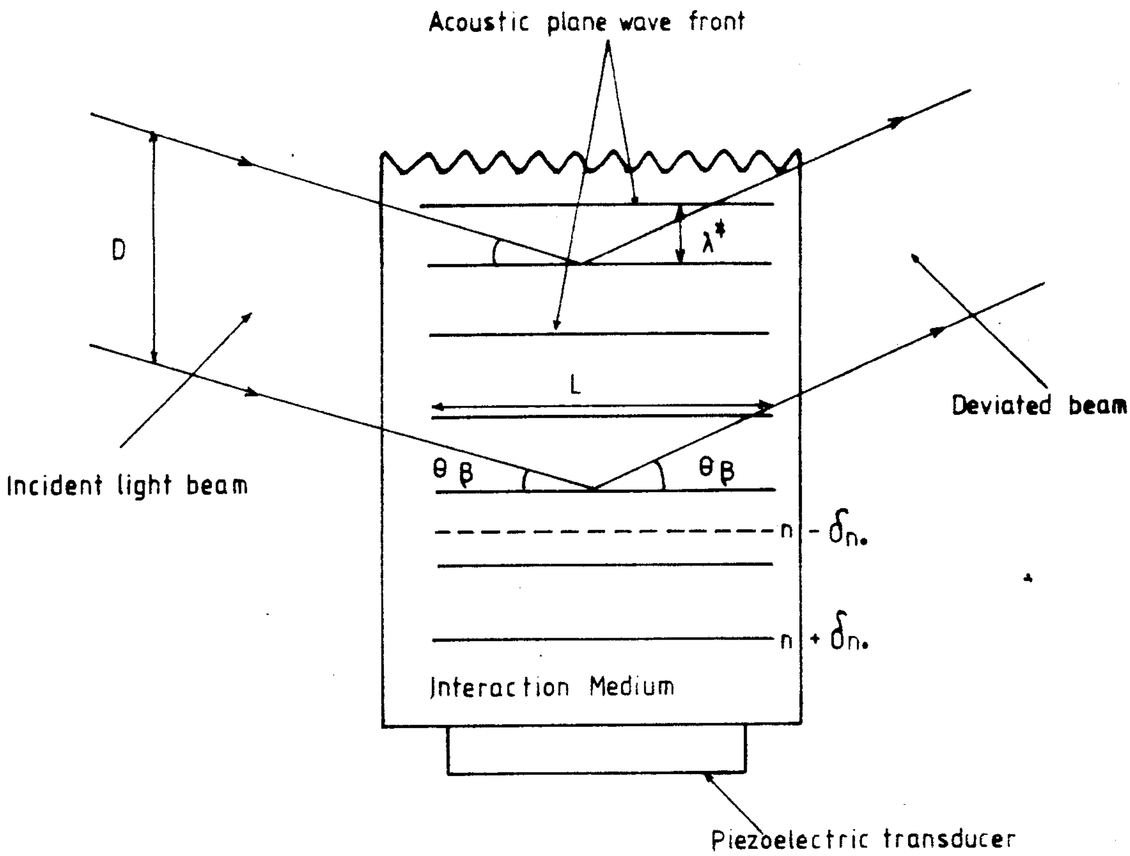

Fig. 2 Standard example of the diffraction of light by acoustic waves.

It can be shown that the proportion of light diffracted by such a grating is related to the parameter ν ;

$$\nu = K\,L\,\delta n_o$$

known as the modulation; δn_o is the amplitude of the variation of the refractive index due, in this particular case, to the photoelastic effect, and $K=2\pi/\lambda$ is the wavevector of the incident light.

To characterise the type of diffraction, we use the dimensionless parameter Q, given by

$$Q = \frac{\vec{K}^{*2} L}{nK} \qquad (2.1)$$

where $\vec{K}^{*}$ is the acoustic wave number, n is the refractive index of the interaction medium. There exist two extreme cases in which analytical solutions to the problem of light diffraction by acoustic waves are found. They are given by

$Q<1$ and $Q>>1$

corresponding to Raman and Nath diffraction, and Bragg diffraction respectively. The difference being that the former is used with normal or quasi_normal incidence. The initial light beam of angular frequency ω and of amplitude, say, 1 is split after interacting with the acoustic waves, into several beams corresponding to different orders of diffraction.

In the Bragg diffraction, there is only a single diffracted beam. The phenomenon only involves one phonon per photon, absorption and emission cannot occur simultaneously, contrary to what happens in the Raman and Nath region. The relation between the associated quantities, the acoustic waves and light are:

$$\vec{K}_d = \vec{K}_i \pm \vec{K}^* \qquad \text{for wave vectors}$$

$$\omega_d = \omega_i \pm \omega^* \qquad \text{for angular frequencies}$$

The i subscript indicates the incident photon, the d subscript the diffracted photon, + sign corresponds to the annihilation of a photon, the - sign to the creation of the same particle. Fig.3. represents the absorption of a phonon. Given that $\omega^* \ll \omega_i$, $\omega_d \simeq \omega_i$, and $|\vec{K}_d| \simeq |\vec{K}_i|$, it can be shown that the quantities above are obeyed for an incidence such that

$$\theta_B = \sin^{-1} \frac{\lambda f^*}{2\nu n} \tag{2.2}$$

θ_B is the Bragg angle and ν is the velocity with which the grating travels parallel to itself.

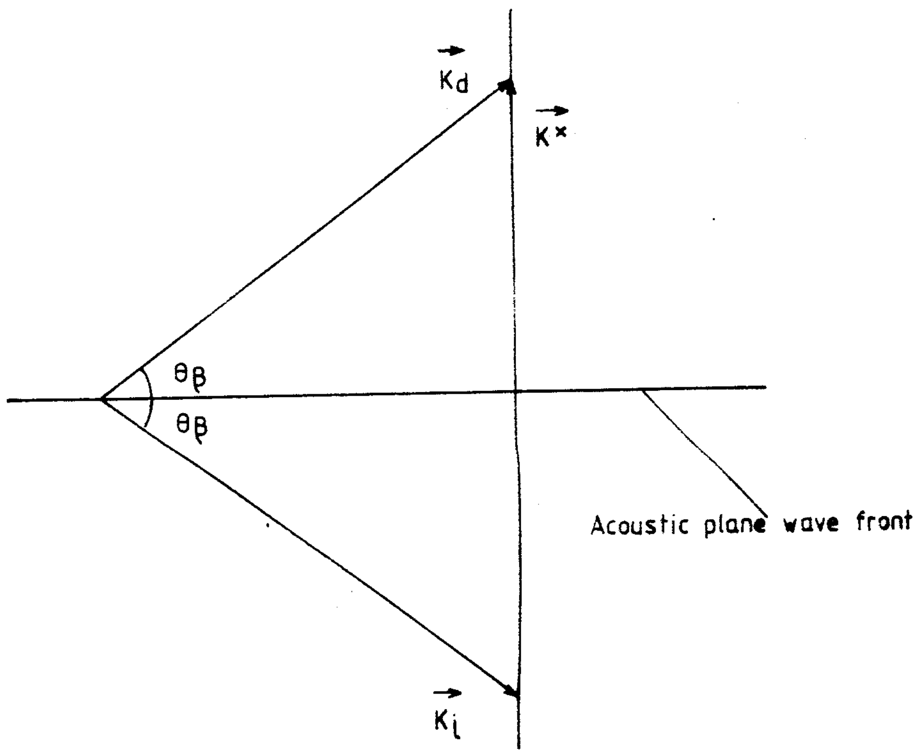

Fig. 3 Bragg diffraction in the case of absorption of phonon in a medium where the refractive index is the same for incident and diffracted waves (the triangle is isosceles).

Where

$\lambda_f^*/2\nu^n << 1$,

$$\Theta_B = \frac{\lambda_f^*}{2\nu^n} \qquad (2.3)$$

The angle of deviation of the light beam is equal to $2\,\Theta_B$(Fig.3. above). Under conditions of incidence given by equation (2.2), the proportion, η, of diffracted light is at a maximum and equal to

$$\eta = \mathrm{Sin}^2\,\nu/2 \qquad (2.4)$$

In reality, acoustic plane wave fronts behave like partially reflecting plane mirrors, of which the reflective power can be varied by varying the acoustic power. The proportion of non_deflected light at the Bragg incidence is obviously equal to $1-\eta$.

To understand the effect of an acoustic pulse, let us suppose that ultrasound or acoustic waves of frequency f^*, no longer continous but in the form of a pulse of width T, is transmitted through the light beam. Suppose for example that we are using the experimental situation where Q>>1 (i.e. in the Bragg case, as used in this work). The maximum efficiency is obtained at the Bragg incidence. At the passage of the acoustic beam across the light beam, a fraction of the light beam is deflected in the form of a light pulse. The light beam is then focussed in the interaction region.

The Acousto_optic Light Deflector_Modulator, used in this experiment, intensity modulated, randomly positioned, or continously scanned a laser light beam at rates up to 40KHz or greater. As a deflector, it had a capability of 100 spot resolution by the Rayleigh criterion for a uniformly illuminated aperture.

The model ADM-40 used was an all solid state acousto_optic light deflector_modulator manufactured from high quality flint glass as the interaction medium with epoxy bonded lead zirconium titanate piezoelectric transducers (section 2.2) for generating the acoustic waves. The usable optical wavelength range is from 420 to 700nm. A light beam entering the acoustic field at nearly normal incidence is deflected at an angle proportional to the acoustic wavelength. A frequency deviation of 20MHz centred at 40MHz can deflect 633nm light through an angle of 3.25

milliradians centred 6.3 milliradians from the undeflected beam. Since the deflector_modulator utilised a "phased array beam steering technique", the deflected light had nearly constant intensity across the deflection angle. Resolution depended on the time bandwidth product which is determined by the length of the optical aperture and bandwidth of the transducers.

When used as an intensity modulator, the RF input frequency to the ADM-40 was held constant while the signal amplitude was varied to produce intensity modulation of the laser beam. The relation between light intensity and applied voltage to the ADM-40, as in any acousto_optic device, is not linear but is

$$I = \sin^2 kV$$

where K is a constant and V is the applied voltage. It is therefore necessary to incorporate a correction circuit in the RF driver to linearize the input_output characteristics if desired. Diffraction efficiency (i.e. the percentage of incident light diffracted into the first main order) is also dependent upon beam diameter. Efficiency is 85% for a 1.4mm diameter beam, and

80% for a 0.65mm diameter beam.

Intensity modulation appears on both the diffracted and undiffracted light, one being the inverse of the other. A 100% depth of modulation could not be obtained with the undiffracted beam, while a ratio in excess of 1000:1 was possible with the diffracted beam at dc.

2.2. PIEZOELECTRIC DETECTION

By definition, piezoelectricity is the electricity (electric charge) generated in a material when mechanical pressure is applied to it (Fig.4.). The opposite effect also occurs; the material changes its physical shape when an electric charge is applied (Fig.5.). The former is referred to as the "generation code" and the latter is called the "motor code".

Among the other important properties of piezoelectric materials are; the "electromechanical coupling",to convert mechanical energy into electrical energy and vice versa and is denoted by a small letter k; the "dielectric constant", which is a measure of the amount of electric charge that it can retain compared to the

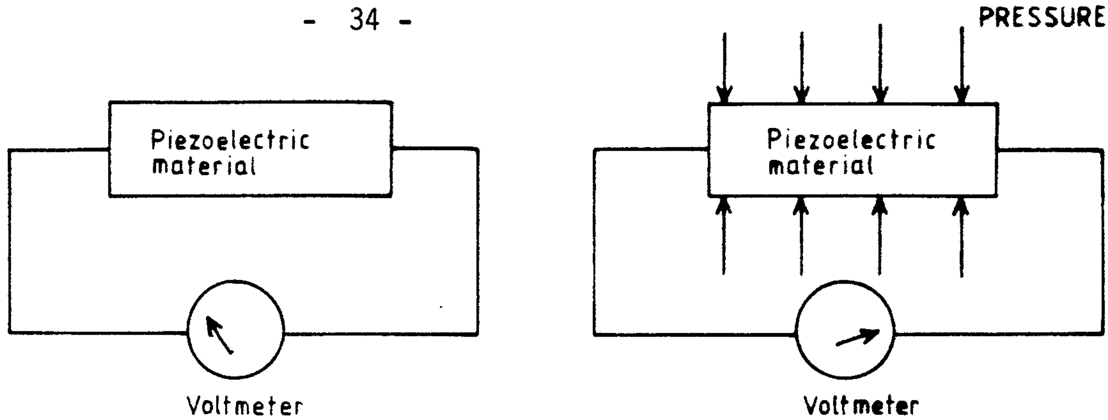

Fig. 4 Voltage generated when pressure is applied

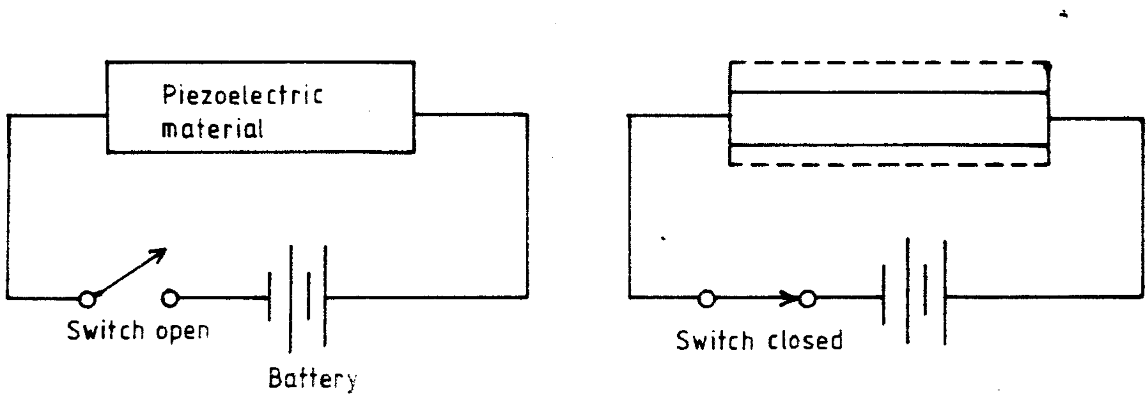

Fig. 5 Change in shape when voltage is applied

charge that would be stored by electrodes of the same area and separated by air as a dielectric (this is analogous to the dielectric constant of a capacitor); the "d constant", a ratio of short_circuit electric charge developed per unit area of electrode to the mechanical stress applied to the piezoelectric element (the d constant will also express the ratio of strain developed along (or around) a specific axis to the value of electric field applied parallel to a given axis). The "g constant" indicates the ratio of electric field generated along a given axis to the stress applied along (or around) a specific axis. This constant also denotes the ratio of strain developed along (or around) a given axis to the electric charge per unit area of electrode perpendicular to a specific axis. For example, g_{33} will provide the ratio of the electric field developed in the material's Z-axis. It will also indicate the ratio of strain developed in Z-axis to the electric charge per unit area of its electrodes.

These properties of piezoelectric materials are very important to understand especially if you are using piezoelectric detection in photoacoustic experiments because they determine how a particular piezoelectric transducer can respond to the level of the generated acoustic waves in the samples under test.

Typically, photoacoustic analysis of solids involves the irradiation of a surface enclosed in a gas_filled cell, by a chopped or modulated beam of light. If the wavelength of the monochromatic periodic light beam entering the cell through a transparent window is one that the sample surface absorbs, the subsequent thermal de_excitation of the energy states excited by the light beam will give rise to pressure oscillations in the surrounding gas, amplitudes of which are proportional to the absorption of the light by the surface. These oscillations are detectable with a microphone also located in the cell, and the resulting signal is amplified and measured by a phase sensitive detector (Fig.6.).

McClelland and Kniseley[16] have proposed an optimal design of a typical Microphone_PAS cell. They have provided a set of experimental data that suggests there is little to be gained in signal to noise ratio and nothing to be gained in photoacoustic signal by working at modulation

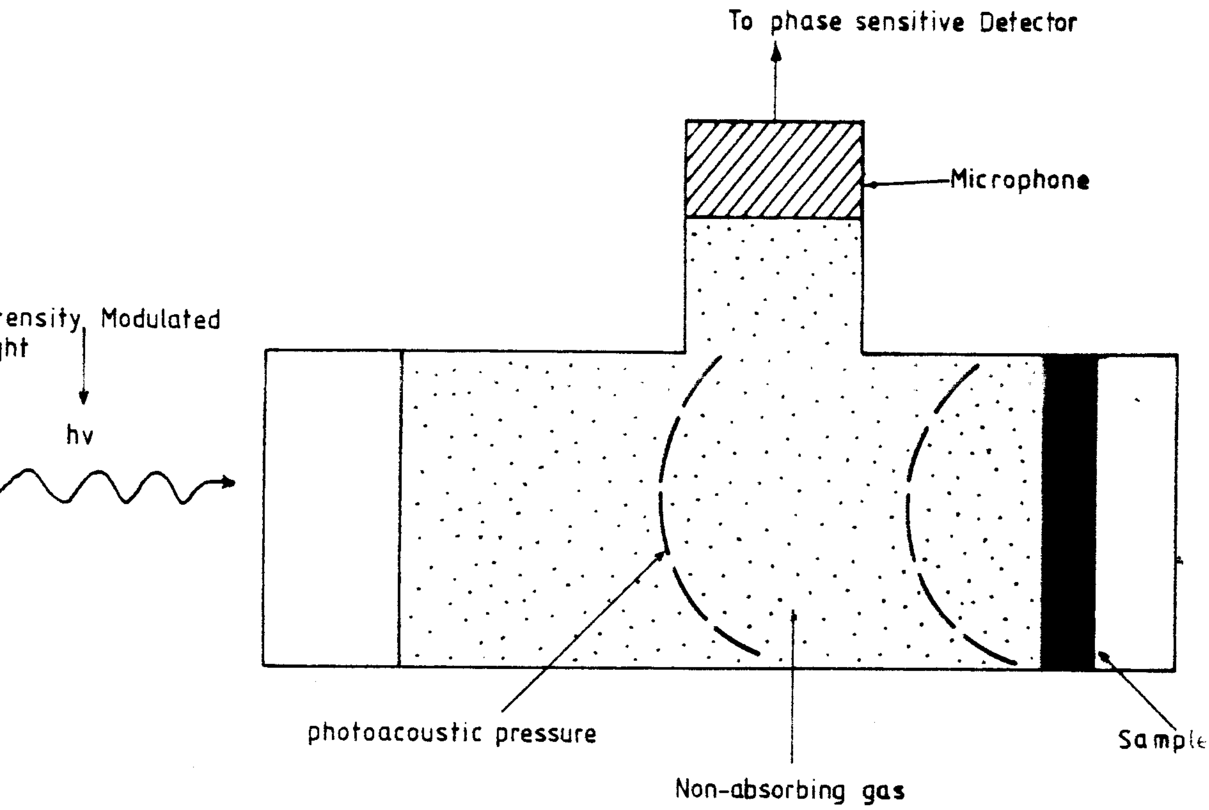

ig. 6 Photoacoustics of a sample using a microphone detector

frequencies exceeding about 50Hz. Clearly, the sensitivity of the microphone to thermal and extraneous enviromental signals mitigates against its use if some other suitable detector is available.Infact the gas_microphone technique works better on gaseous and powder samples than on bulk solid samples or liquids where the surface_to_volume ratio is not large because the heat transfer from sample to the gas in the cell is considerably reduced. For bulk solids, a more efficient means for measuring the amount of internal heating is depicted in Fig.7.

A piezoelectric transducer (e.g. a Lead Zirconium Titanate(pzt) ceramic) is in direct contact with the solid bulk sample, which is illuminated with an intensity modulated light. Because a piezoelectric transducer is being used, modulation frequencies can be in the MHz range, if desired. The internal heating caused by the absorption of the incident light will result in both thermoacoustic and thermoelastic signals being generated in the sample. If the piezoelectric detector is more than a few thermal diffusion lengths away from the light absorbing region, then only the thermoelastic signals will

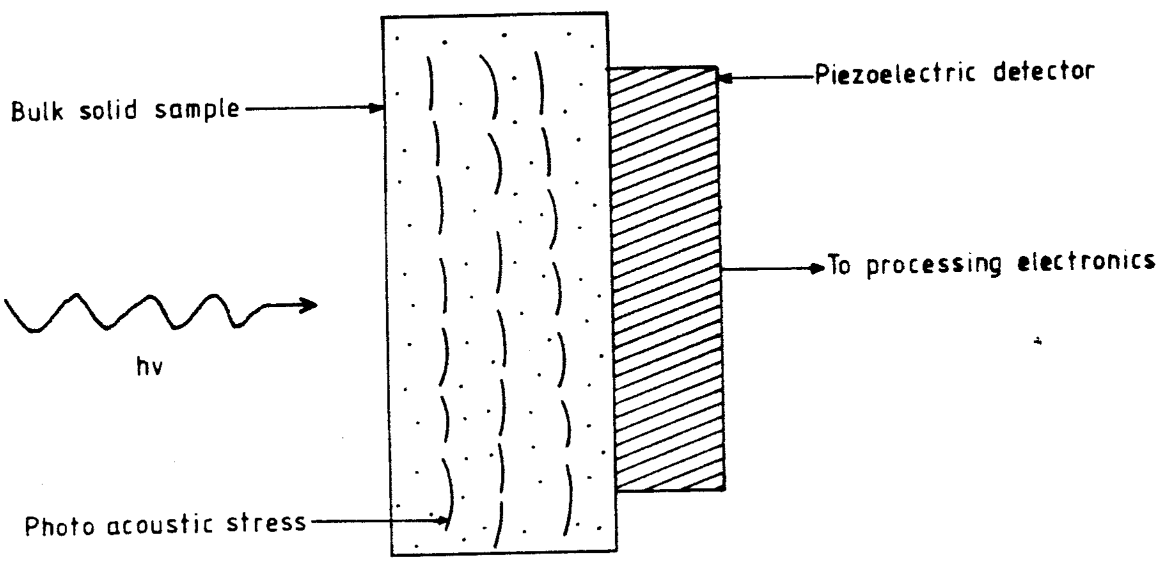

Fig. 7 Photoacoustics of a bulk solid sample using the piezoelectric method.

be detected.

The voltage, V, produced by the piezoelectric transducer due to a stress σ in the bulk sample is given by[17]

$$V = g\ t\ k\ \sigma$$

where g is the piezoelectric constant mentioned earlier, t is the thickness of the piezoelectric crystal and k is the electromechanical coupling between the sample and the piezoelectric transducer.

For a finite solid sample, the stress σ is usually composed of both longitudinal and shear stresses having different boundary conditions at the surfaces of the sample. A careful analysis of this situation indicates that the piezoelectric signal tends to decrease with modulation frequency at low frequencies (f<1MHz), then decrease more slowly or even increase at higher frequencies (1MHz<1GHz), and then finally decrease rapidly at very high frequncies (f>1GHz). The actual frequency behaviour is dependent on the optical, geometrical, thermal and elastic properties of the sample, although for most situations, the strongest photoacoustic signals occur at low modulation frequncies, where easily detectable signals of 1-10 μV can be obtained from piezoelectric ceramics where samples of up to 1 cm^3 in volume absorb a few milliwatts of optical power.

The use of piezoelectric detectors for measuring optically generated acoustic signals offers greater versatility than microphonic techniques. Sensitivity similar to that attained with microphones is possible, but without the physical vunerability of a microphone. Piezoelectric transducers can perform satisfactorily in either an ac mode or an impulse mode offering additional freedom to the experimenter. Furthermore, the feasibility of detecting only the acoustic wave rather than its thermal effects permits direct analysis of phase angle relationships and facilitates identification of the signal source. In addition, a piezoelectric system is better suited for photoacoustic imaging and microscopy since the sample need not be limited in size or shape, as it does not need to be enclosed in a small sealed gas_cell.

2.3. THE PHASE SENSITIVE DETECTOR (PSD)

The most common source of noise encountered in low level measurements is Johnson noise caused by the random motion of thermally agitated electrons in resistive materials. Johnson noise is "white noise", that is, its root mean square value per unit bandwidth is constant from dc to frequencies extending into the infra_red. Other noise sources include discrete interfering signals, flicker noise, and shot noise. These noise sources all have one thing in common, they obscure a signal of interest, cause measurement errors or make a measurement impossible. However, with phase sensitive detection, a small signal can be measured that might be 50dB or more below the noise level.

Phase sensitive detection is a technique which measures the mean amplitude of ac signal (V_S) often buried in noise and is normally used in applications where the signal results from the application of an ac stimulus to a system under test (as done in this work). Since photoacoustic measurements involves such signals, phase sensitive detection is up to now, the most reliable technique used and a clear understanding of this method is very important.

The Phase Sensitive Detector (PSD) is a phase sensitive ac voltmeter that responds to input signals at or near the frequency of a reference signal. To better understand the operation of PSD, a diagram of a typical design is shown in the Fig.8. below.

In order for the PSD to operate a reference voltage which is coherent with the signal of interest is required. Therefore a voltage derived from the stimulus (which may be mechanical, optical, magnetic, etc.) is applied to the reference input. The output comprises a dc voltage proportional to the required component of the signal and also ac components due to noise. The ac components due to noise are filtered with the low_pass filter of variable time constant.

The input signal, after being amplified (and perhaps filtered), is applied to one input of a PSD. The reference signal is processed by a reference circuit which, in this case, can change the phase but not the frequency of the reference signal (the stimulus), and is applied to the other

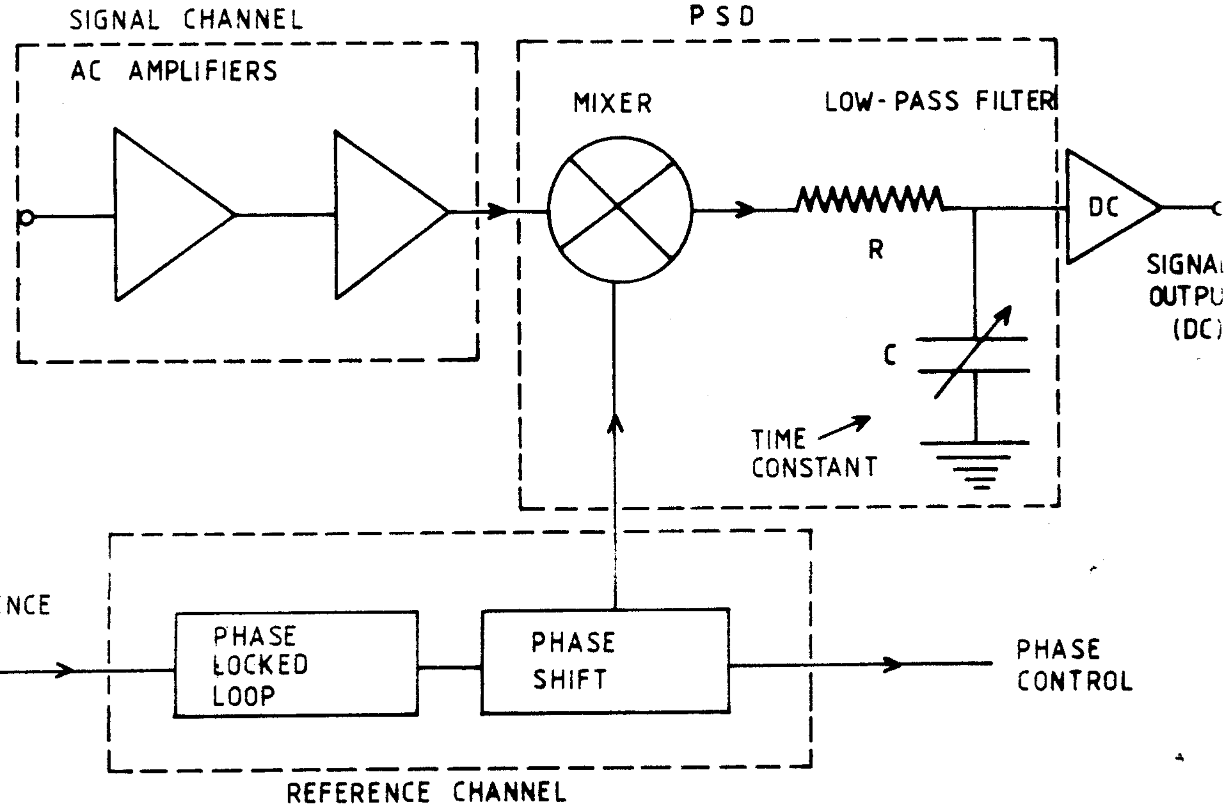

Fig.8. Typical Phase Sensitive Detector design.

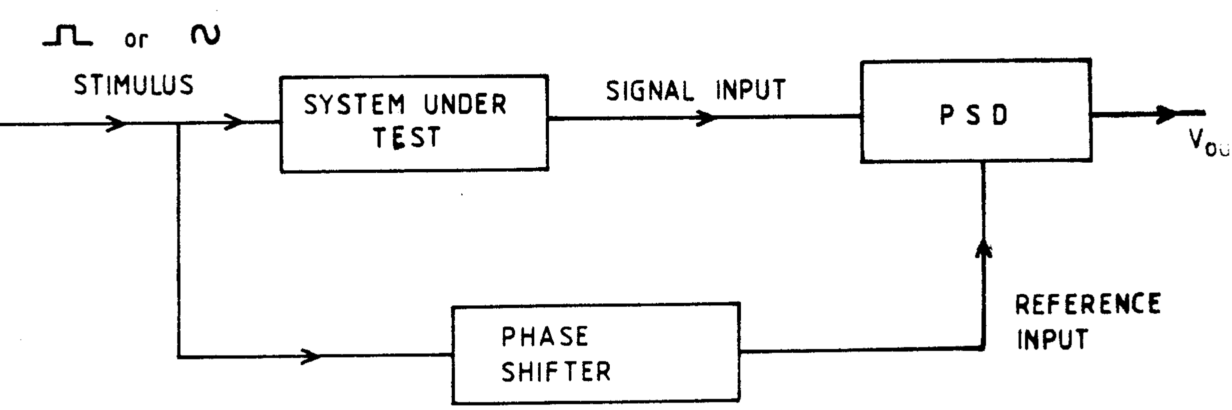

Fig.9. AC stimulus applied to a system under test in a PSD measurement.

input of the PSD.

Most PSDs work on the principle of the synchronous switch (Fig.10.). The signal is periodically switched into the load resistor, the frequency and phase of the switching operation being determined by the reference voltage.

It is clear that if the signal and reference voltage have the same frequency and phase, the voltage appearing across the load resistor will have the form shown below (Fig.11.)-there should be noise in this signal, of course. That is, the switch will act as a halfwave rectifier for signals of the same frequency and phase as the reference. If the signal is in quadrature with the reference, the corresponding waveform will be as shown in Fig.12. and rectification will not occur. Intermediate phase angles give a dc output proportional to the in_phase component.

Thus, a signal input which is exactly the same as the reference input results in an output at "zero Hz" or dc. It can be seen that the dc component easily passes through the output low_pass filter. This action may be summarized as follows:

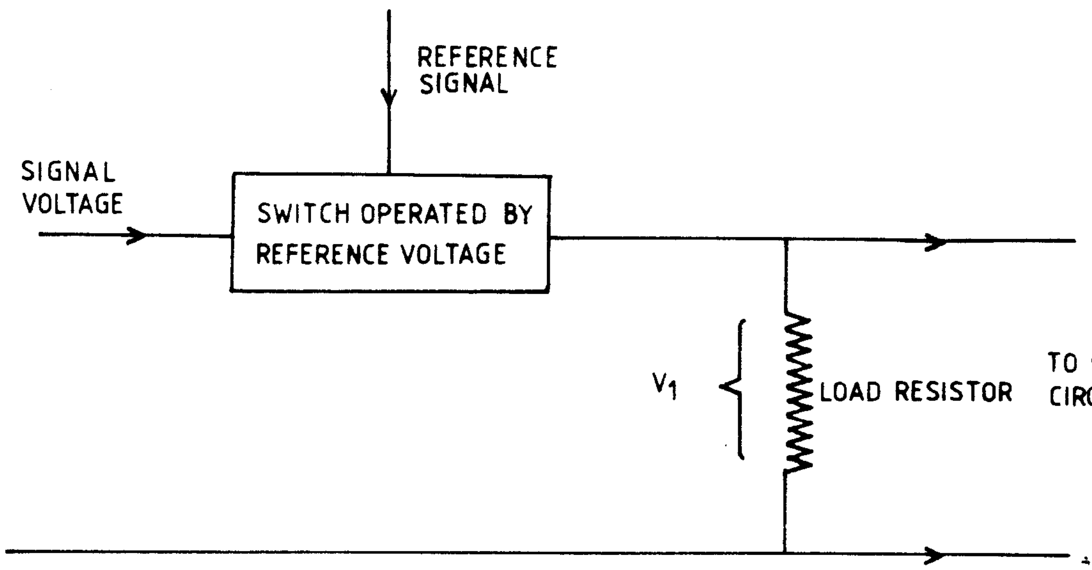

Fig.10. Diagram representing the principle of the synchronous switch.

Let the reference voltage be $V_r \sin\omega t$.
Then if the signal voltage is $V_s \sin(\omega t + \alpha)$
a dc voltage will appear across the
load resistor proportional to $V_s \cos\alpha$.

Signals at any frequency other than the reference (and its odd harmonics) cannot yield dc output. Signals at nearby frequencies, however, produce relatively low frequency components that can pass through the low_pass filter with little attenuation. The output filter includes a wide range of time constants so that the rejection of all unwanted signals including Johnson noise, can be made arbitrarily large. Thus the response of the system to noise will depend on the time constant T_o of the dc measuring circuit and the PSD acts as a selective rectifier of bandwidth $1/T_o$ radians per second.Thus by use of the appropriate time constant the desired bandwidth for the entire system may be obtained.

It should be noticed that the PSD also responds with reduced sensitivity to noise bands centred on frequencies which correspond to odd harmonics of the reference frequency; with a flat noise spectrum this effect reduces the effective signal_to_noise ratio by 1dB especially when they

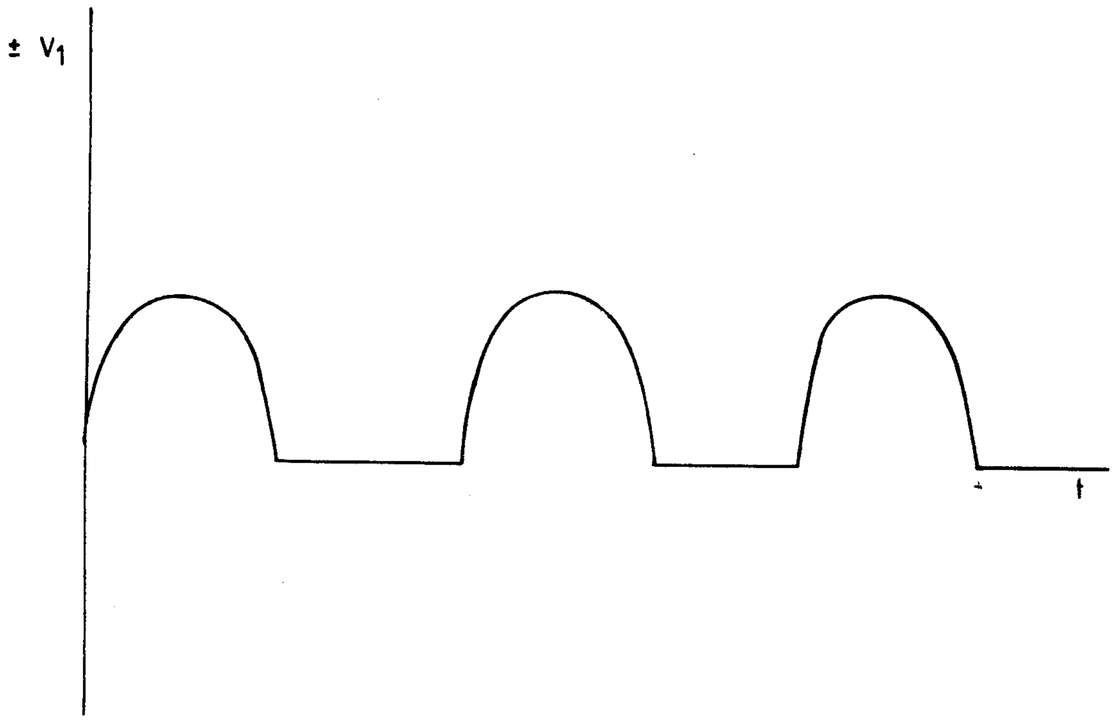

Fig.11. Output voltage appearing across the load resistor when the input signal is in phase and has the same frequency with the reference voltage.

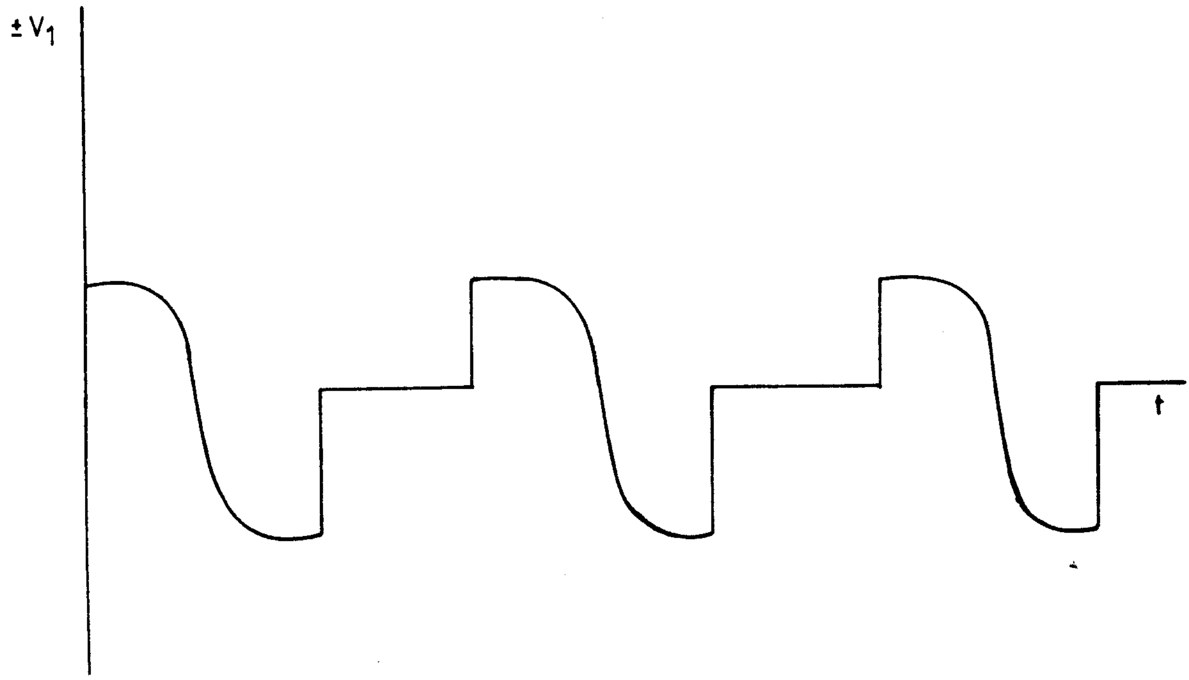

Fig.12. The output signal when the input signal is 90 out of phase with the reference signal.

are used in chopped light experiments.

Actually the PSD shown in Fig.10. is unbalanced. A better performance can be obtained by using a balanced switching circuit with a two_way switch connected to two load resistors, as shown in Fig.13. The voltage across the two load resistors obtained with an in_phase signal are shown below. It can be seen that the balanced PSD gives a full wave rectification rather than half wave rectification, into the dc measuring device.

Mathematically, the operation performed by the PSD corresponds to multiplying the signal input voltage by a square wave, that is by a function $F_1(t)$ where

$$F_1(t) = \mathrm{Sin}\,\omega t + \frac{1}{3}\,\mathrm{Sin}\,3\omega t + \dots\dots\dots\dots$$

so that if the signal voltage itself is $V_S F_S(t)$, the output is

$$V_1 - V_S = V_S\,\overline{F_1 F_S}$$

where the average time is T_o , the time constant.

Thus the PSD performs a Fourier analysis of $F_S(t)$ and extracts the components corresponding to $\mathrm{Sin}\,\omega t$ (and its odd harmonics). In short, it

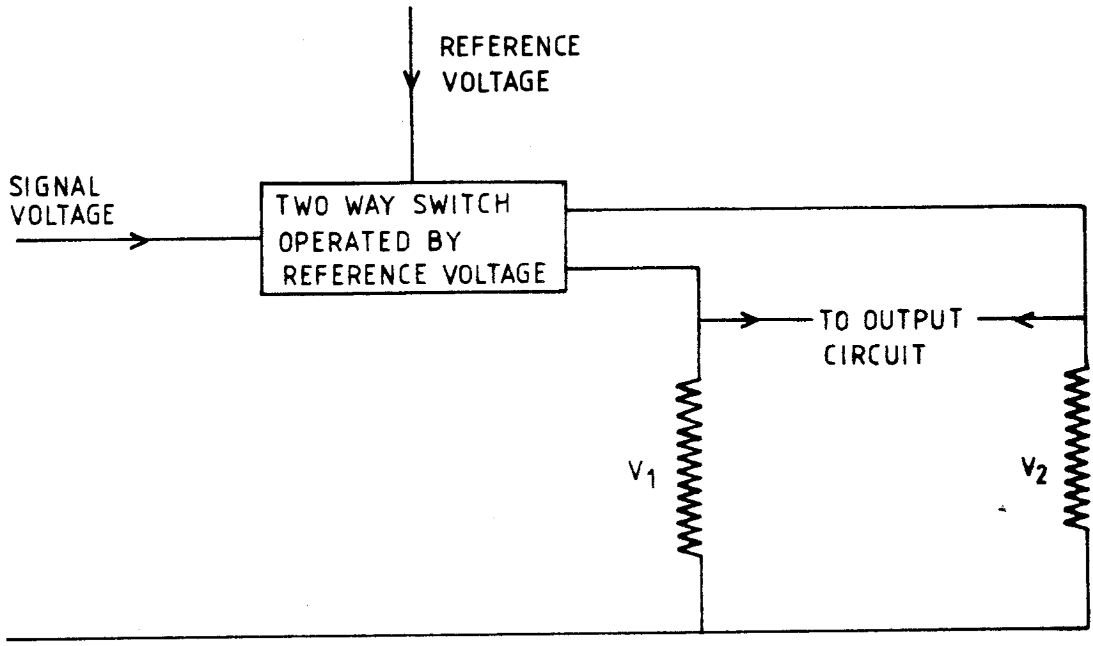

Fig.13. A balanced version of the PSD showing the synchronous switching circuit which incorporates two load resistors and a two_way switch.

extracts a signal from noise by multiplying the signal input voltage with the reference and then filtering the product with a low_pass filter of time constant T_o .

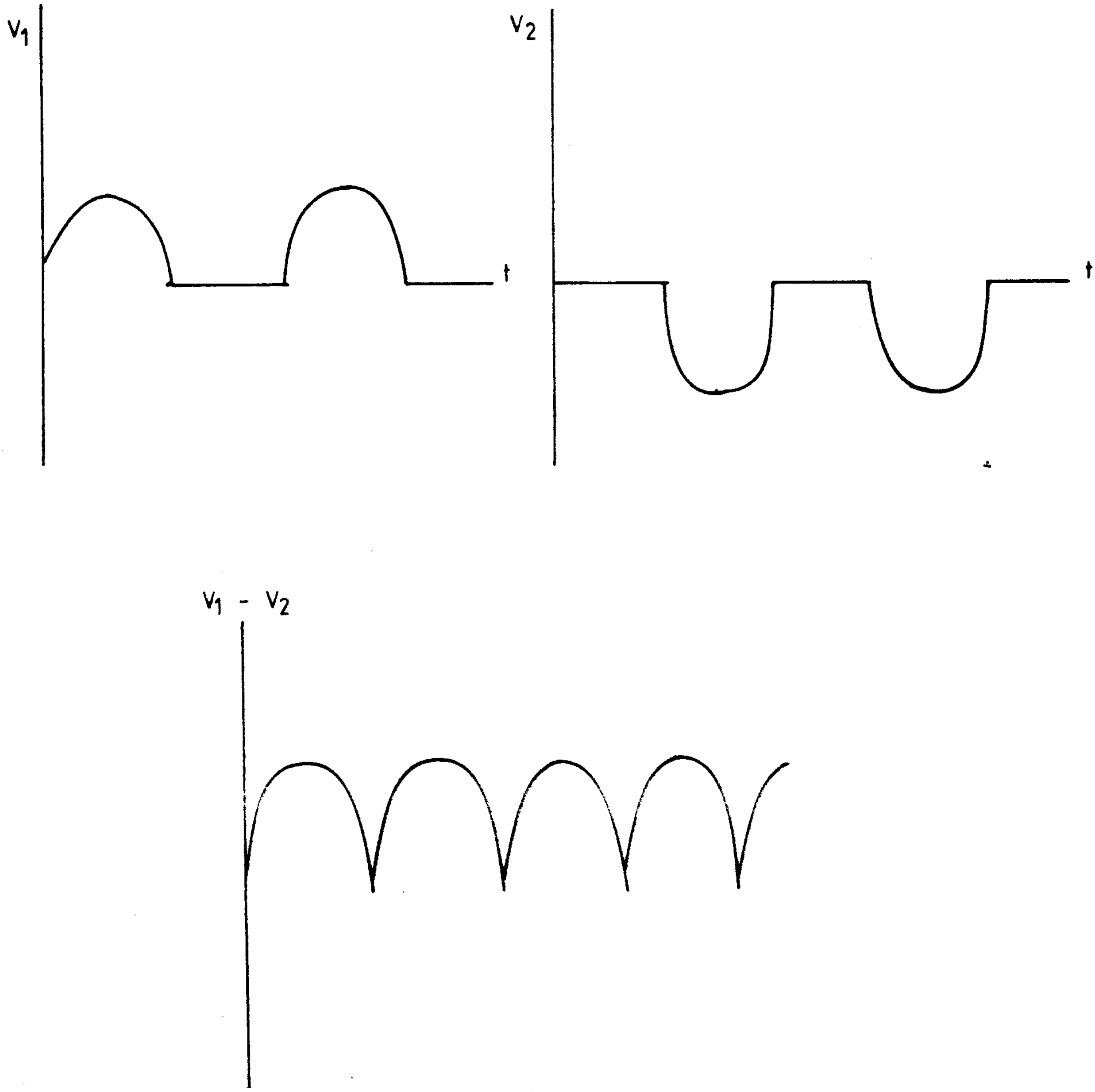

Fig.14. Voltage across the two load resistors obtained with in_phase signals. Notice the resultant full_wave rectification.

CHAPTER THREE

THE EXPERIMENTAL WORK

3.1. CALIBRATION OF THE APPARATUS

In most experiments involving noise in the signals of interest, it is quite important that some sort of calibration of the detection system is carried out so as to be able to clearly differentiate between the various signals that may arise. In this photoacoustic experiment, as in other similar works previously carried out, there is quite a substantial noise level encountered which tries to obscure and distort the true results. As a result, a calibration of the detection and measuring systems is very important if the results are to be understood and explained well. Besides, it also helps the experimenter to know the behaviour of the measuring system one is using.

3.1.1. CALIBRATION OF THE PHASE SENSITIVE DETECTION SYSTEM

This simply involved taking a 2Volts p_p signal from a signal generator and attenuating it by

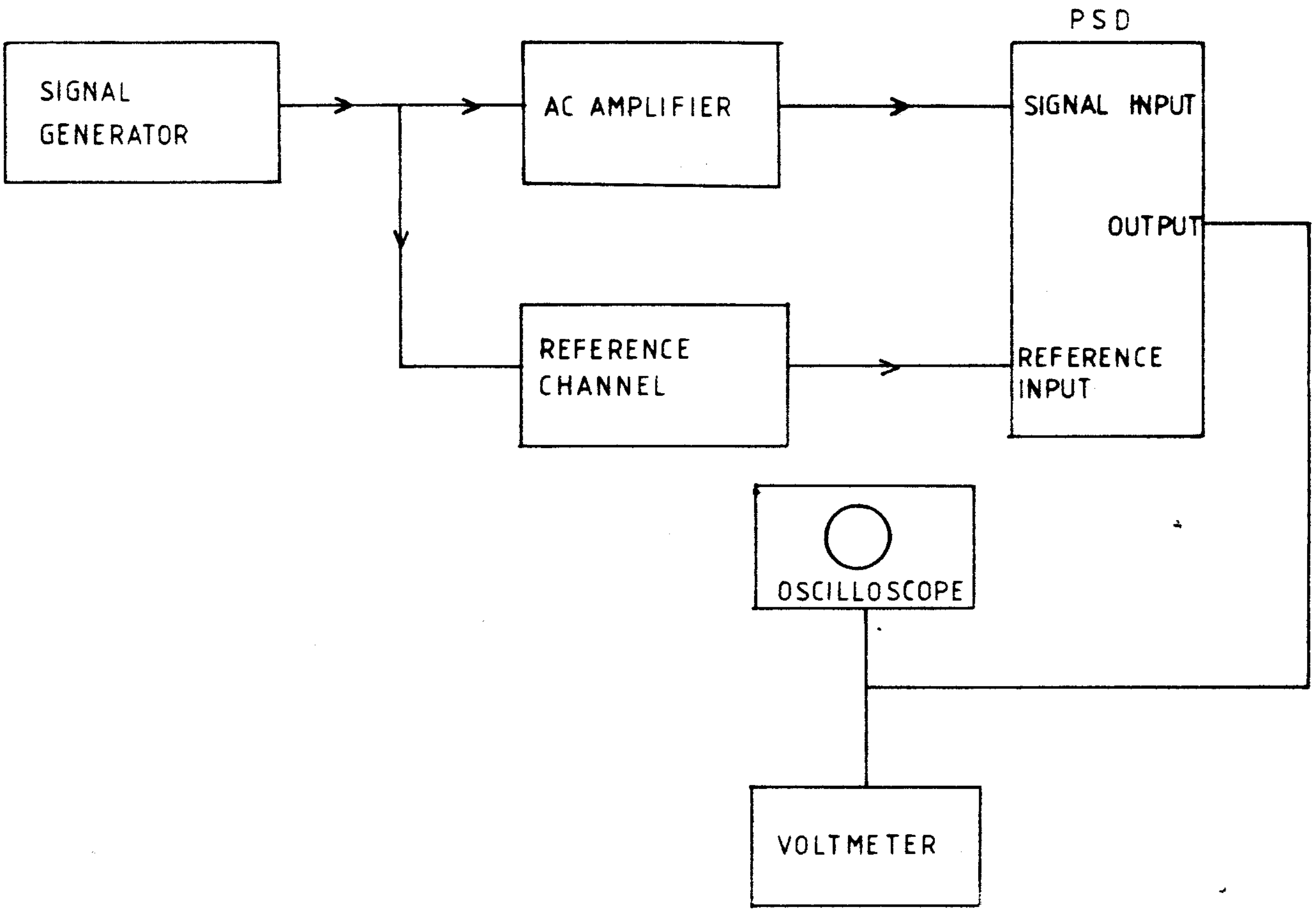

Fig. 15 Block diagram of the Calibration of the phase Sensitive Detection system

about 80dB. This attenuated signal is passed through the AC amplifier, from the amplifier into the phase sensitive detector where it was mixed with the reference signal from the signal generator through the reference channel (shown in Fig.15.). The output of the PSD, as the range of frequencies from 10Hz-1MHz was being scanned, was monitored using an oscilloscope and a digital voltmeter. Then the plot of the output voltage against the frequency was drawn, as shown in the Figures 16(a) and 16(b), which correspond to two different filter choices of the measuring system. In both cases, it can be seen from the calibration curves that the output tails off around 100KHz as it approaches 1MHz. This is as expected because at 1MHz, the output is attentuated by 3dB from its maximum value, that is according to the characteristics of the PSD. The fall at low frequencies is also due to the filter characteristics of the measuring system, where the 50Hz components are filtered out of the input signal giving out a reduced output voltage. In the remaining region, the output signal is constant as there should not be any variations of the output with frequency since the amplitude of the input signal remains constant. It is just the frequency

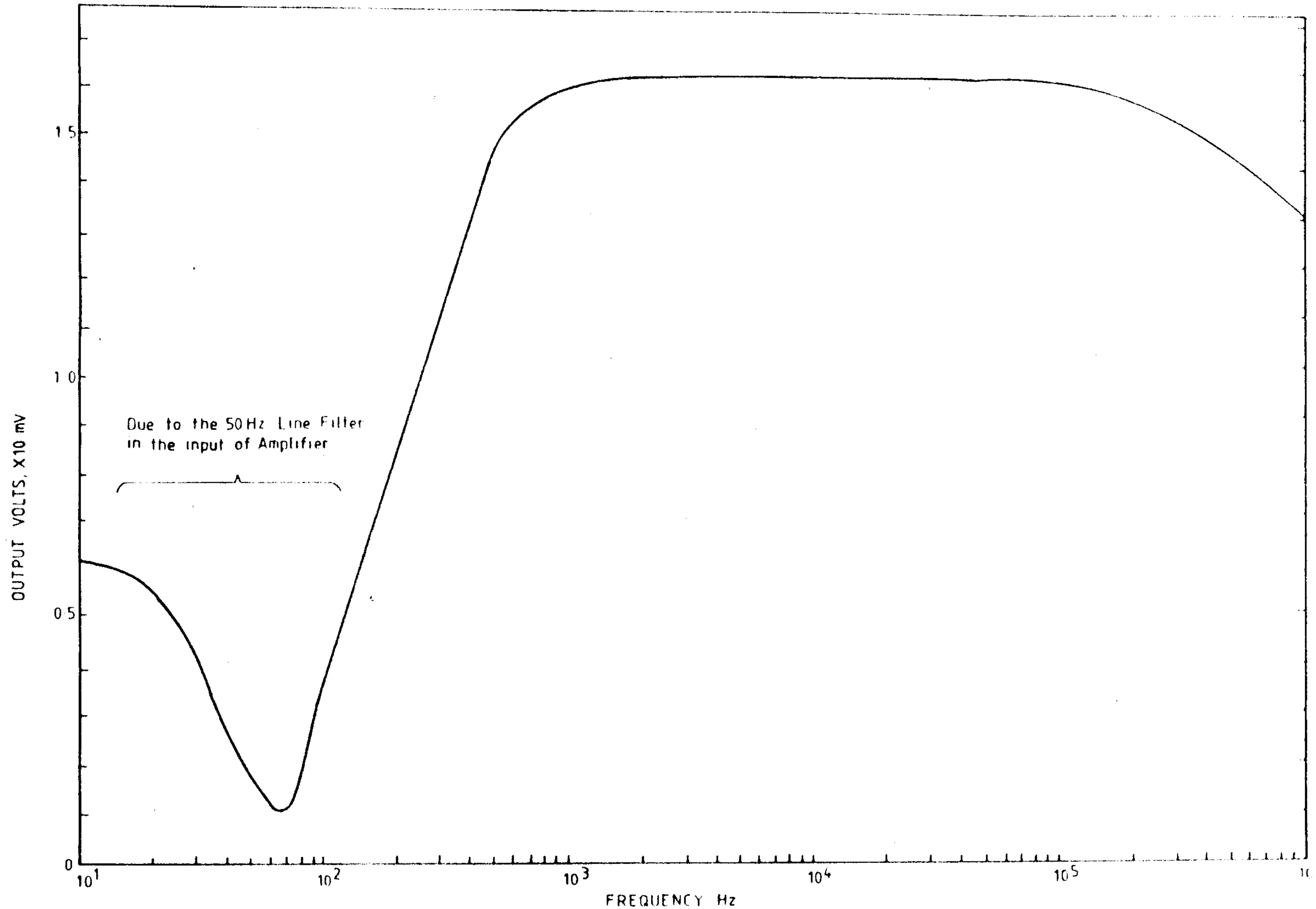

Fig 16(a) Calibration Curve of the PSD system with Line Reject Filter on

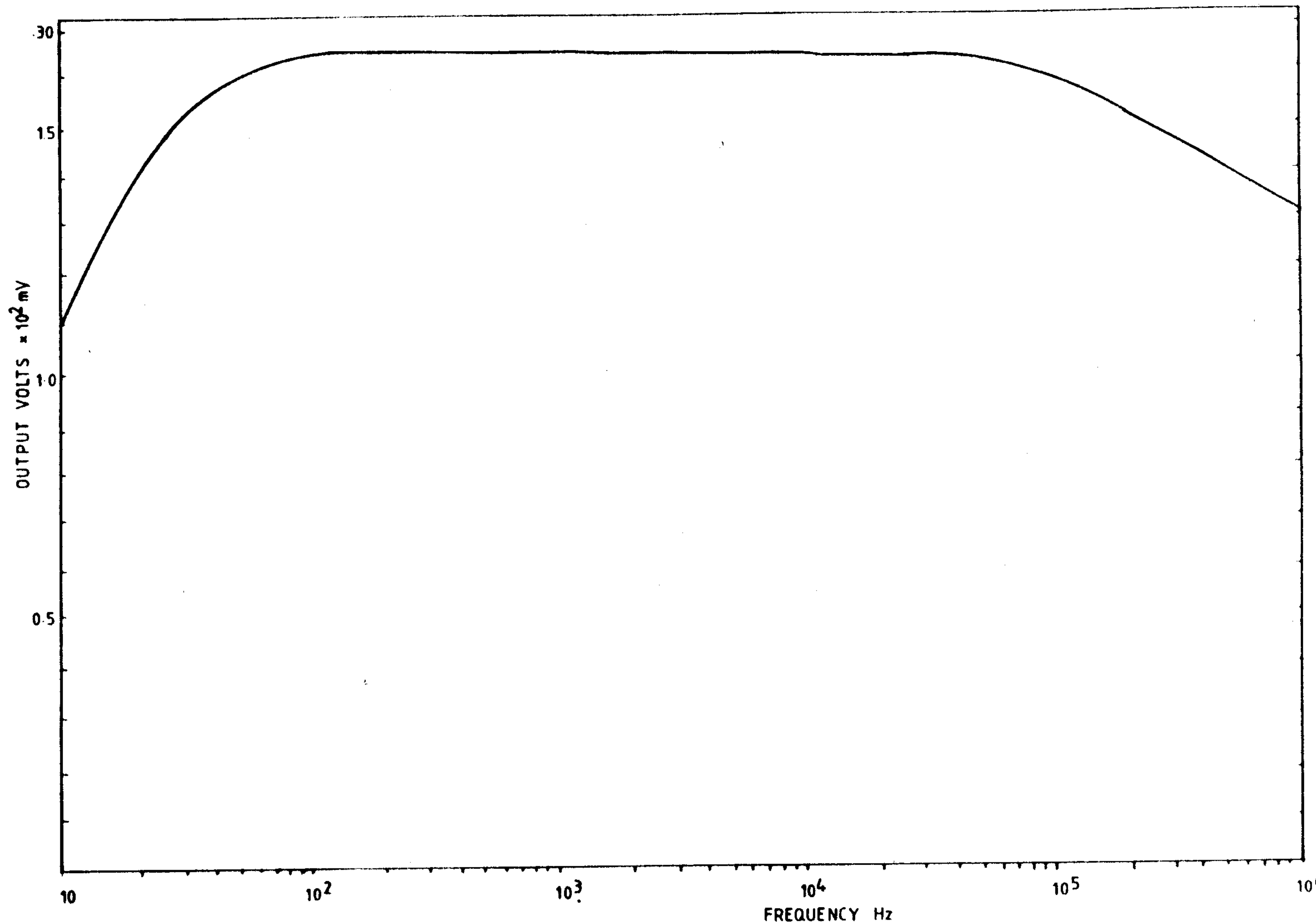

Fig. 16(b) Calibration curve of the PSD system with LRF off.

we are changing, for both the reference and the input signals to the PSD, otherwise the amplitudes remain constant. So we do not expect any variations in the output signal. In other words, the inputs to the PSD (both the input and reference signals) are of constant amplitudes and are in phase so that we expect the output to be the same in the remaining region.

3.1.2. CALIBRATION OF THE PIEZOELECTRIC TRANSDUCER

This was done by illuminating a disc of the lead zirconium titanate (pzt) piezoelectric transducer with a modulated laser beam, thereby inducing some stress_strain flunctuations in the pzt. Due to these stress_strain flunctuations there is a voltage generated across the parallel faces (section 2.2.) of the disc, which was collected by wires (leads) attached to the faces.This output voltage from the transducer was then passed through the amplifier and into the phase sensitive detector. From the PSD, the output was monitored by the oscilloscope and a voltmeter. At each modulation frequency, starting from 10Hz up to 1MHz, the output voltage was recorded and the calibration curve obtained as shown in Fig.17.

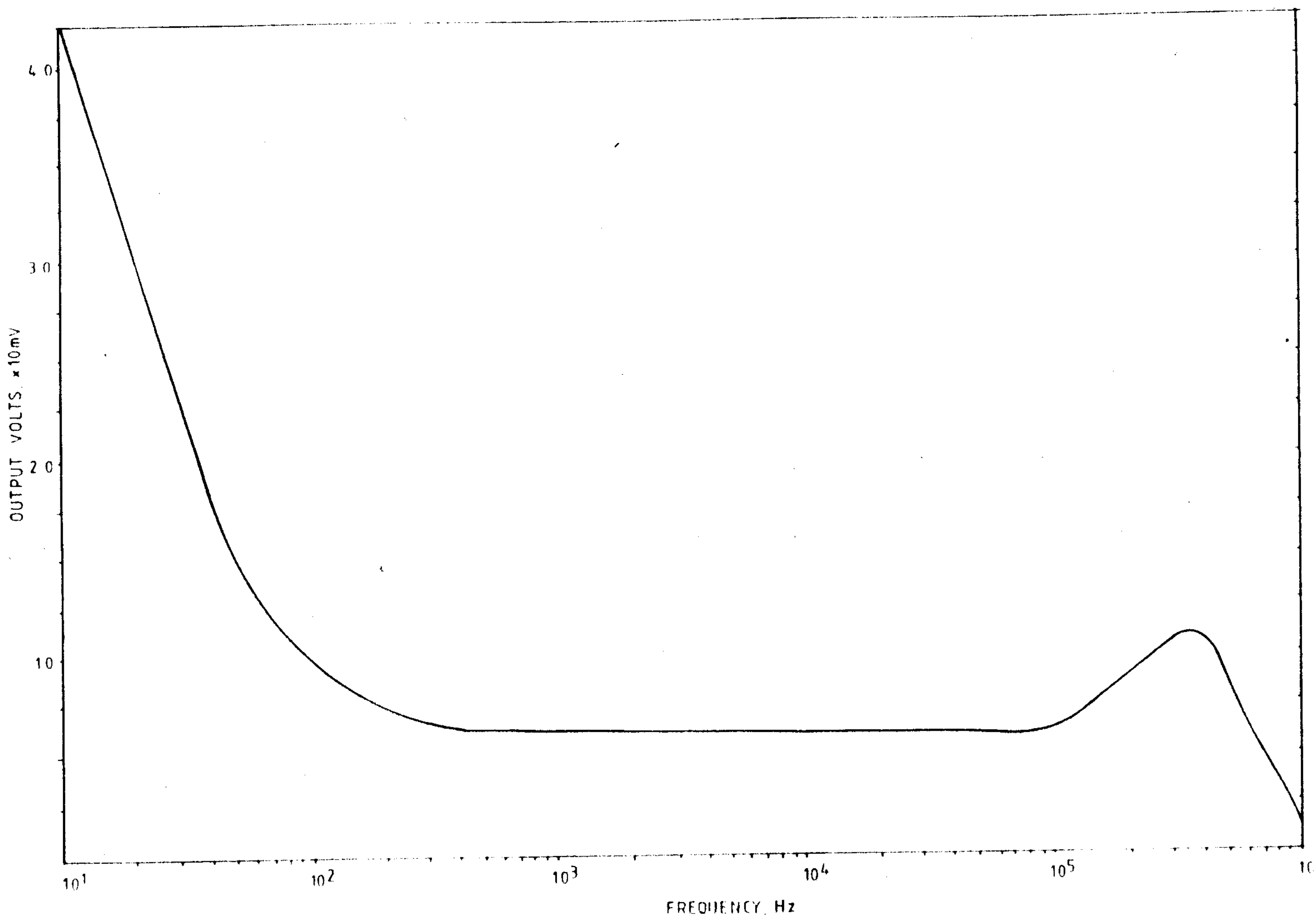

Fig 17 Calibration curve of the transducer

In this experiment, an intensity modulated optical beam is focussed across the surface of the opaque transducer resulting in localized periodic heating from the absorption of the incident beam. From the basic equation governing this thermal diffusion[18],

$$\frac{\partial T(x,t)}{\partial t} = D\,\frac{\partial^2 T(x,t)}{\partial x^2} \tag{3.1}$$

the solution to this periodic thermal diffusion equation appropriate to this situation will be a thermal wave, so damped that in most cases, it propagates not more than a wavelength, although this is also dependent on the modulation frequency. $D = k/c\rho$ where k is the thermal conductivity, c is the specific heat capacity, and ρ is the density. T is the periodic temperature distribution which is different at different distances from the absorbing surface and at different times, t.

This equation can be satisfied by a product solution $T(x,t)=f(x)g(t)$. At any particular plane, say x_1, and under any steady state varying heat supply for example, $e^{j\omega t}$, the temperature at x_1 must vary periodically (but not necessarily in phase) with the heat supply. That is

$$\frac{\partial T}{\partial t} = j\omega T$$

so that equation (3.1) becomes

$$D\frac{\partial^2 T}{\partial x^2} = j\omega T$$

or

$$\frac{\partial^2 T}{\partial x^2} - j(\omega/D)\,T = 0 \qquad (3.2)$$

This is identical to the skin effect situation encountered in electromagnetic waves. From equations (3.1) and (3.2)

$$f(x) = A\,e^{-\frac{1}{\sqrt{2}}(1+j)(\omega/D)^{\frac{1}{2}}x} \qquad (3.3)$$

so that

$$T(x,t) = A\,e^{-(\omega/2D)^{\frac{1}{2}}x}\,e^{j[\omega t-(\omega/2D)^{\frac{1}{2}}x]} \qquad (3.4)$$

Equation (3.4) represents a thermal wave of wave number $\vec{K} = (\omega/2D)^{\frac{1}{2}}$ and wavelength λ given by

$$\lambda = 2\pi/\vec{K} = (8\pi^2 D/\omega)^{\frac{1}{2}} = (4\pi D/f)^{\frac{1}{2}} \qquad (3.5)$$

where f is the modulation frequency, $\omega/2\pi$.

The amplitude of the temperature oscillation diminishes like $e^{-\vec{K}x} = e^{-x(\omega/2D)^{\frac{1}{2}}} = e^{-(2\pi x)/\lambda}$

thus falls more rapidly for large frequencies, just as shown in Fig.17. At a distance of one wavelength, the amplitude is reduced by a factor of $e^{-2\pi} = 0.0019$, so that the waves are very strongly attenuated. Since the wavelength falls as we approach 1MHz, we expect the temperature wave to propagate into the sample through a very short distance. For the piezoelectric transducer used here, $K=1.5Wm^{-1}\,{}^{o}C^{-1}$, $\rho=7.5\times10^{3}\,Kgm^{-3}$, and $C=420JKg^{-1}$ so that at high frequencies, the wavelength is of the order of a few microns. These parameters are important especially when measurements by periodic methods are being performed. In most ordinary cases, observations will be made over a distance of the order of a wavelength and this somehow determines the frequency one can adopt for modulating the beam.

The pzt output is determined by the total strain and this will be different for different heat (temperature) distributions. The more the waves penetrate into the solid, the more these pressure effects in the sample and hence the larger the voltage generated. In addition to the large distances penetrated by the thermal waves at low frequencies, the period of heating is such that the sample has enough time to expand and contract, thus giving out large voltages. The rapid fall suggests the effect of changing the temperature distribution (although the estimated thermal depth is only 0.1mm at 10Hz). The flat bit is when effectively only one face is heated and the pzt output is caused by the bending effect.

The peak in the calibration curve was due to the resonant response of the pzt transducer itself. It was observed to exhibit resonance at 200KHz, 300KHz, and 500KHZ. From its specifications, its resonance is at 1MHz although it was found to show resonance at these frequencies. The reason for its not showing any resonance at 1MHz could be because of the limitation in the operating frequency of the PSD system (section 3.1.1). This limitation, as we will see later, proved to be a severe drawback in carrying out measurements at higher frequencies (MHz range) as the phase sensitive detector system only worked well up to 500KHz.

The other important point to note is that there is a progressive lag $\vec{K}x = (\omega/2D)^{\frac{1}{2}}x$, in the phase of the temperature wave. This lag will increase with frequency. The temperature flunctuations such as the positions of the maxima and minima of temperature are propagated into the solid with velocity $(2D/\omega)^{\frac{1}{2}}$.

3.1.3. CALIBRATION OF THE SEMICONDUCTOR

An attempt was also made to calibrate the semiconductor; that is illuminating the GaAs wafer with a modulated beam of light and then looking at the response of the GaAs at different modulation frequencies. This was done in order to obtain some idea, though crude, as to what frequency we might need to modulate the beam,that can give us some maximum response from the samples.

The GaAs wafer was first mounted on an aluminium buffer rod (instead of cementing it directly on the pzt)[21], at the back of which a pzt piezoelectric transducer was then cemented to detect the acoustic signals from the semiconductor, passing through the aluminium rod. From the pzt, the signal was processed through the amplifier and phase sensitive detector and then measured by a voltmeter and an oscilloscope. The GaAs sample was 0.20mm thick and 1cm in diameter, with the polished surface being illuminated.

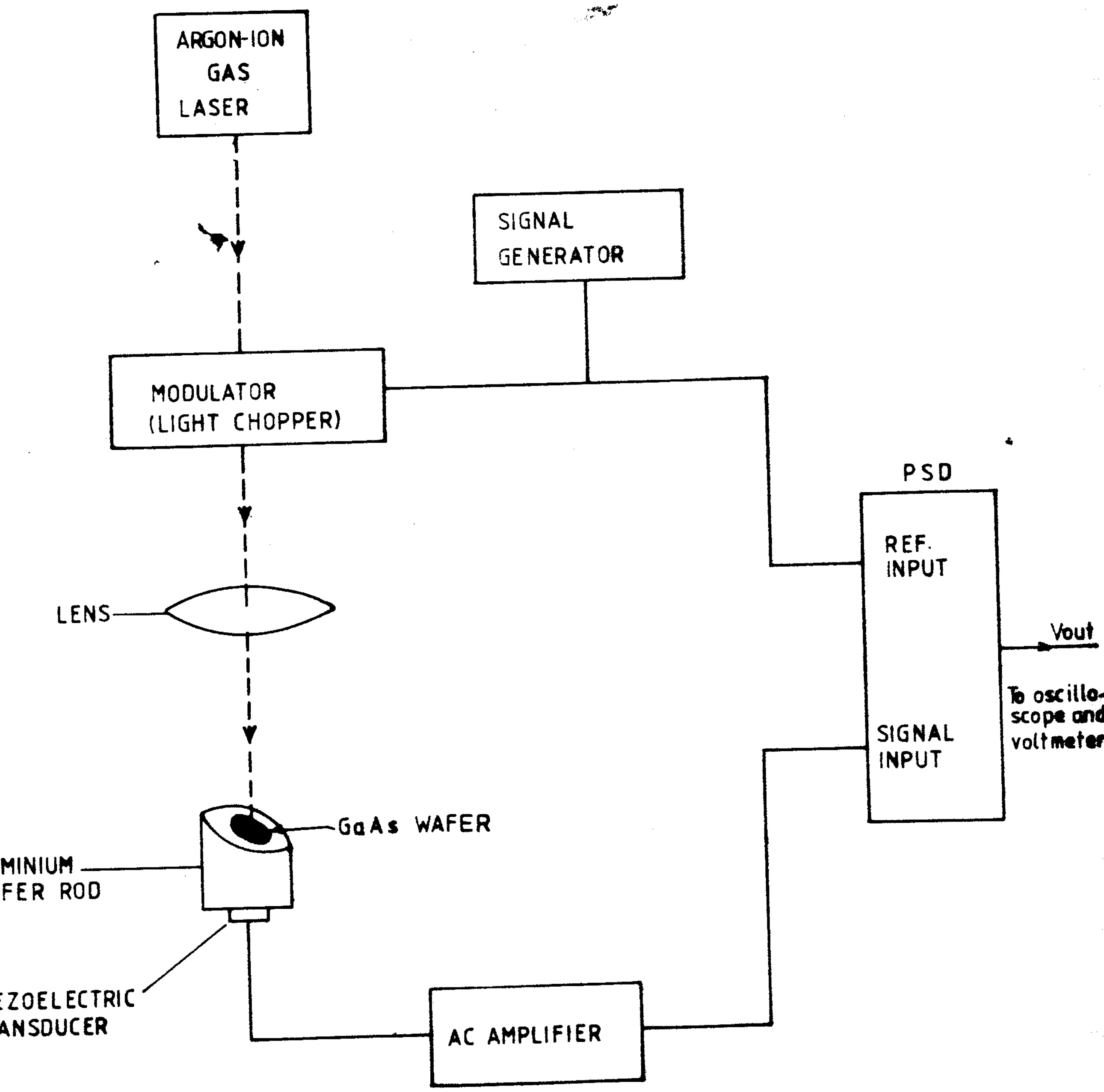

Fig. 18 Schematic of the experimental arrangement for calibrating the Semiconductor (GaAs)

In this experiment, the illumination causes the injection of carriers (electron_hole pairs) in the semiconductor, which as seen in section 1.2. constitutes a strain in the solid. The periodic photogeneration of these carriers causes periodic stress_strain variations in the sample which results in acoustic waves being propagated through the material. We therefore should expect response of the pzt to be proportional to the number of generated carriers. The more the generated carriers, the larger the stress_strain flunctuations and hence the larger the output signal recorded by the detection system.

A plot of the magnitude of the generated acoustic signal versus the frequency of modulation is shown in Fig.19. The shape of the curve seems to suggest that there is a better output response in the frequency range of 1KHz-10KHz, an indication that modulation frequencies in this range produce a larger strain effect in the sample, due to greater numbers of generated carriers. Infact we can get some idea of the true input voltage to the PSD system; that is the pzt output, by making use of the calibration curve of Fig.16(b). For example, true input at 200Hz

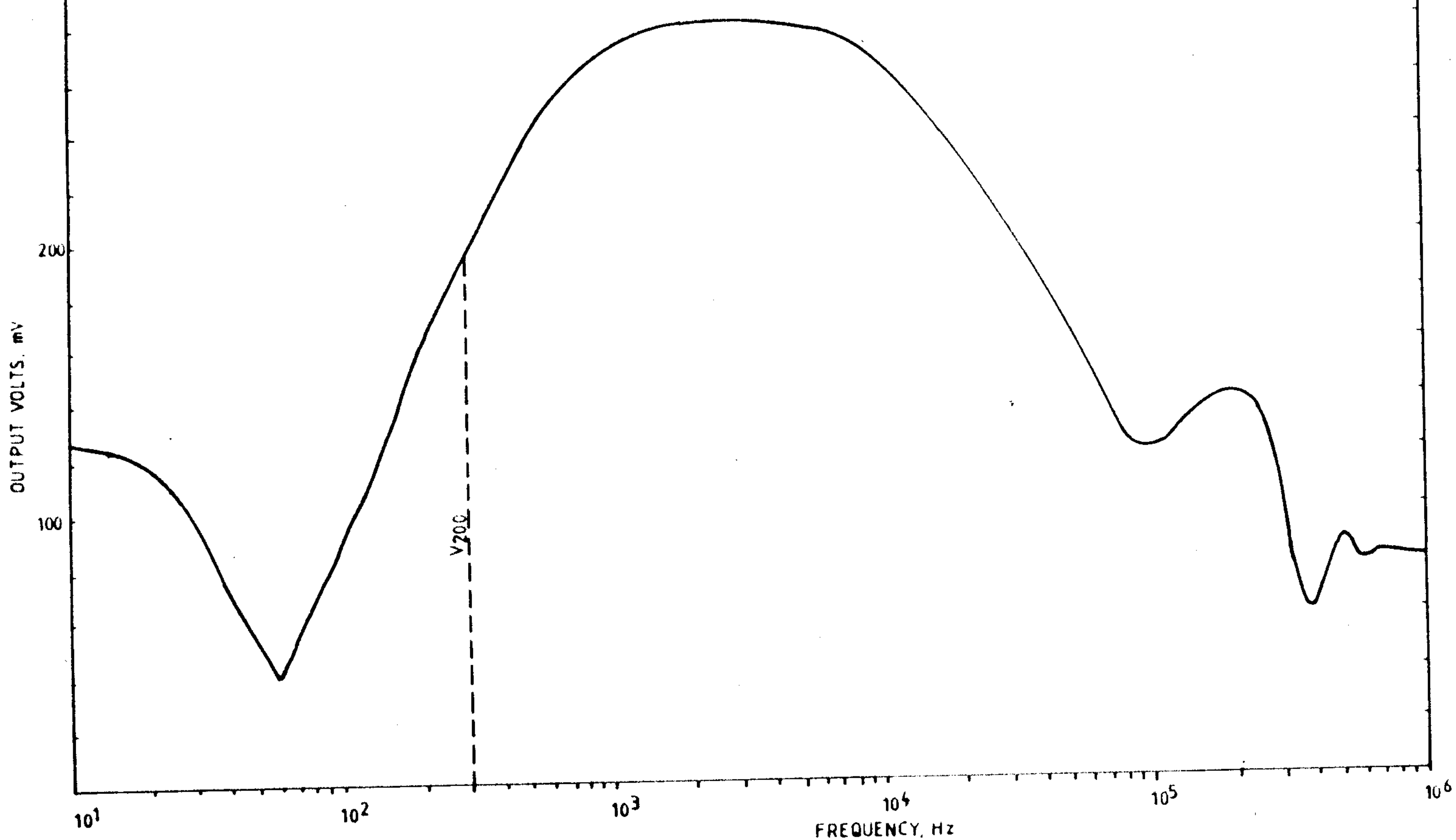

Fig. 19 Calibration curve of the semi conductor (GaAs)

$$= V_{200} \times \frac{V_{10KHz} \text{ on Fig.16(b).}}{V_{200} \text{ on Fig.16(b).}}$$

where V_{10KHz} is at the region where the response is flat, etc. We also note that the behaviour below 1KHz is very largely determined by the 50Hz filter characteristics shown in Fig.16(b). However, to draw a more quantitative conclusion from this measurement, the process of the generation of carriers must be investigated in greater detail.

In a semiconductor an electron_hole pair is produced when an electron passes from the valence band to the conduction band provided $h\nu > E_g$ where, $h\nu$ is the photon energy and E_g is the band gap. In the experiment the wavelength of light used is 514.5nm which corresponds to $h\nu = 2.42eV$, and E_g for GaAs is about 1.47eV. The reverse process is the recombination of the electrons and holes. The time rate of this process increases with the rate at which electrons and holes meet. The number of recombinations per unit time and volume is then proportional to the concentration of electrons, n, and to that of holes, p. On the other hand, the production rate of electro_hole pairs per unit time and volume is independent of the number of electrons and holes and depends only on the width of the forbidden gap.

If we introduce (by means of this light) into the semiconductor densities n and p greater than the equilibrium values n_o and p_o, the electrons and holes will recombine and tend to restore the system to equilibrium. The results in Fig.19. may be explained in terms of the rate of change of the number of carriers. In a simpler form we have,

$$\begin{pmatrix}\text{Variation of}\\ \text{the number}\\ \text{of carriers}\end{pmatrix} = \begin{pmatrix}\text{Generation}\\ \text{rate of}\\ \text{carriers}\end{pmatrix} - \begin{pmatrix}\text{Recombination}\\ \text{rate of}\\ \text{carriers}\end{pmatrix} - \begin{pmatrix}\text{Other losses}\\ \text{of carriers}\end{pmatrix}$$

Assuming that the dominant source of losses is through the recombination process, we can neglect the last term and write

$$\frac{\partial n(t)}{\partial t} = -\frac{n(t)}{\tau} + N_0 e^{j\omega t} \qquad (3.6)$$

where n(t) is the density of carriers (say, electrons) τ is the carrier lifetime and taking $N_0 \exp(j\omega t)$ as our generation rate. If we assume the solution n=Nexp(mt), and substitute this into equation (3.6), we obtain

$$N\,(mt + 1/\tau)\, e^{mt} = N_o\, e^{j\omega t} \qquad (3.7)$$

For these two sides to be equal, we should have $m=j\omega$ and $N = N_o/(m + 1/\tau)$, or

$$\left| n(t) \right| = \left| \frac{N_o}{j\omega + 1/\tau} \right| \qquad (3.8)$$

so that the density is related to the frequency of modulation. N_o is determined only by the beam intensity. The magnitude of the output depends both upon the amplitude of the variation of the generated carriers, and upon the distribution of the carriers in the semiconductor, necessarily associated with the diffusing heat (temperature) wave and affected by the thickness of the sample.

Now, from the magnitude of the carrier density (equation (3.8)), if $1/\tau \gg \omega$ or $\omega\tau \ll 1$, that is very short lifetime << period, then $n \propto N_o\tau$, is independent of ω and we have simply a constant number of carriers. But there will be frequencies high enough that $\omega \gg \frac{1}{\tau}$ and then $n \propto N_o/\omega$, so that the effect decreases almost linearly with ω (Fig.20.). The bending effect is

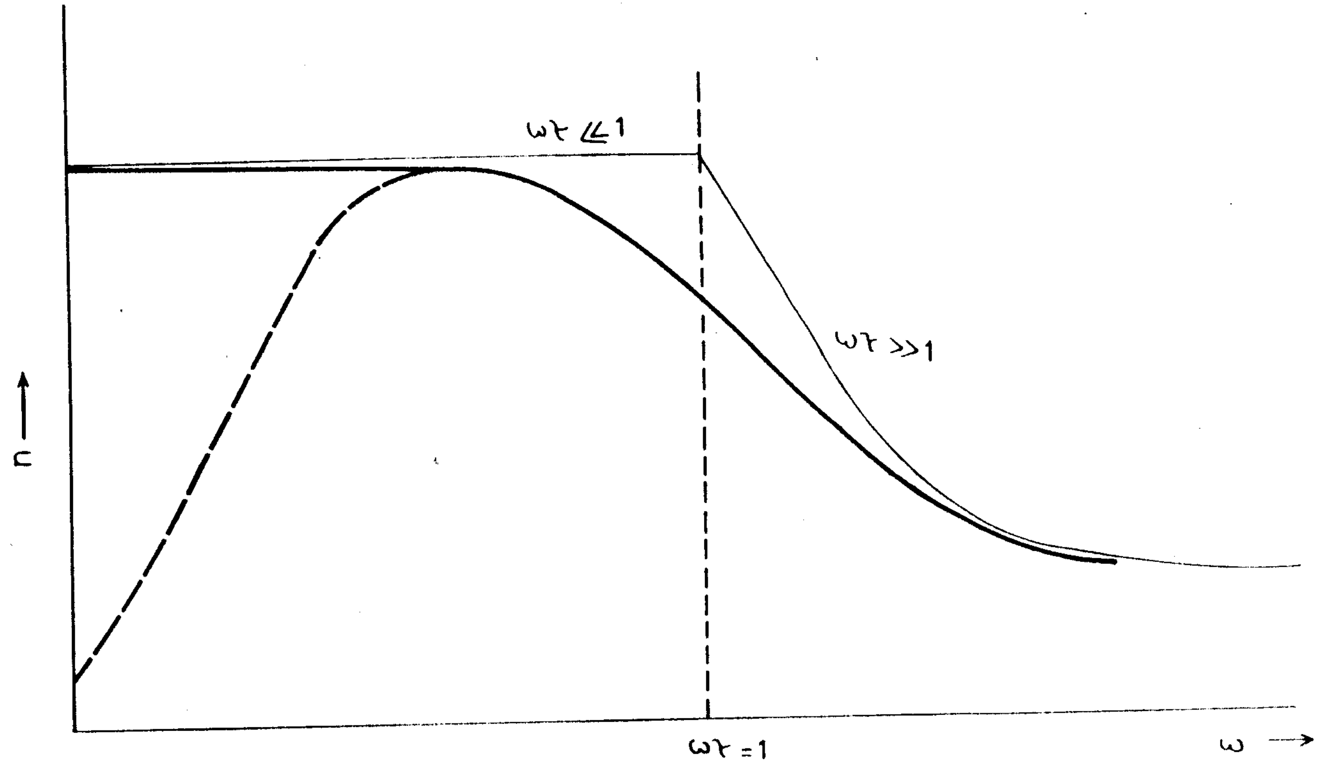

Fig. 20 A Schematic representation of the distribution of Carriers with frequency as deduced from equation (3.6)

more dependent on the skin depth, δ, (that is, the depth of penetration of the temperature wave into the sample). Since $\delta \propto 1/(f)^{\frac{1}{2}}$, the skin depth becomes extremely small as the frequency is increased. The bending effect will be a maximum when d (the thickness of the sample) is effectively half wavelength long but this will be an almost indistiquishable peak superimposed upon the asymptotic value for $\delta \ll d$. (See solid bold curve in Fig.20.).

If these two pencil responses are multiplied, that is,the frequency variation and the skin effect, we obtain almost what Fig.19. shows, especially at high frequency (as we approach 1MHz). The falling off at low frequencies is difficult to justify though this could be due to the 50Hz Line Reject Filters at the input of the measuring system which filters off the 50Hz components of the signal and thus attenuates the output. In addition to this, there is the effect of rapid recombination compared to the slow generation of carriers at these low frequencies, since the lifetime of the carriers is much smaller than the rate at which carriers are being generated. For the GaAs sample used

$$\left|n(t)\right| = \left|\frac{N_o}{j\omega + 1/\tau}\right| = \frac{N_o\tau}{\sqrt{2}}$$

when $\omega\tau = 1$. Assuming that the output voltage is linearly related to $n(t)$, we can deduce from the measurements of Fig.19., that $\omega\tau = 1$ at $\omega \simeq 2\pi \times 20 \times 10^3$ hence $\tau \simeq 80\mu s$ so that the experimental results are roughly in agreement with the theory within experimental errors.

The reason for using the aluminium buffer rod is to separate the semiconductor from the polarized pzt transducer, and avoid any possible heating of the transducer, though it is noted from the calibration curve (Fig.19.) that the resonance has shifted a little presumably because it is stuck on the aluminium. It will also be noted that the wafer is mounted at 30 with respect to the transducer. This has been done to enhance the detection of the longitudinal acoustic waves generated, as has been shown in previous works[19,20,21]

3.2. SAMPLES AND MATERIALS

Two semiconductor samples were selected for investigation to represent a range of direct and indirect band_gap semiconductors. These were thermally oxidised wafers of <100> cut silicon and GaAs, of diameter 2.5cm and thickness 0.41mm and 0.43mm, respectively. The silicon was doped with an order of 10^{13} P atoms/cm^3 while the GaAs was undoped. Each had half of its polished surface (which was being illuminated) coated with Chromium, Cr, metal about 700-800Å thick for GaAs and 850-880Å for silicon. The coating was simply to serve as a source of heating for the semiconductor while in the bare region, both thermal heating and generation of carriers due to the light beam will occur. The thicknesses of the metallic coating as measured for each sample are shown in Fig.21. and 22., taken at different points of the samples, and it can be seen that there is a large variation in the thickness of GaAs than in silicon. The wafers were then mounted onto an aluminium buffer rod (section 3.3) the back of which was stuck a 1MHz lead zirconium titanate (pzt) piezoelectric transducer.

Fig.23. shows the configuration of the transducer. The point to note is that the aluminium, as mentioned earlier (section 3.3) serves as a buffer region to separate the semiconductor from the pzt transducer in view of

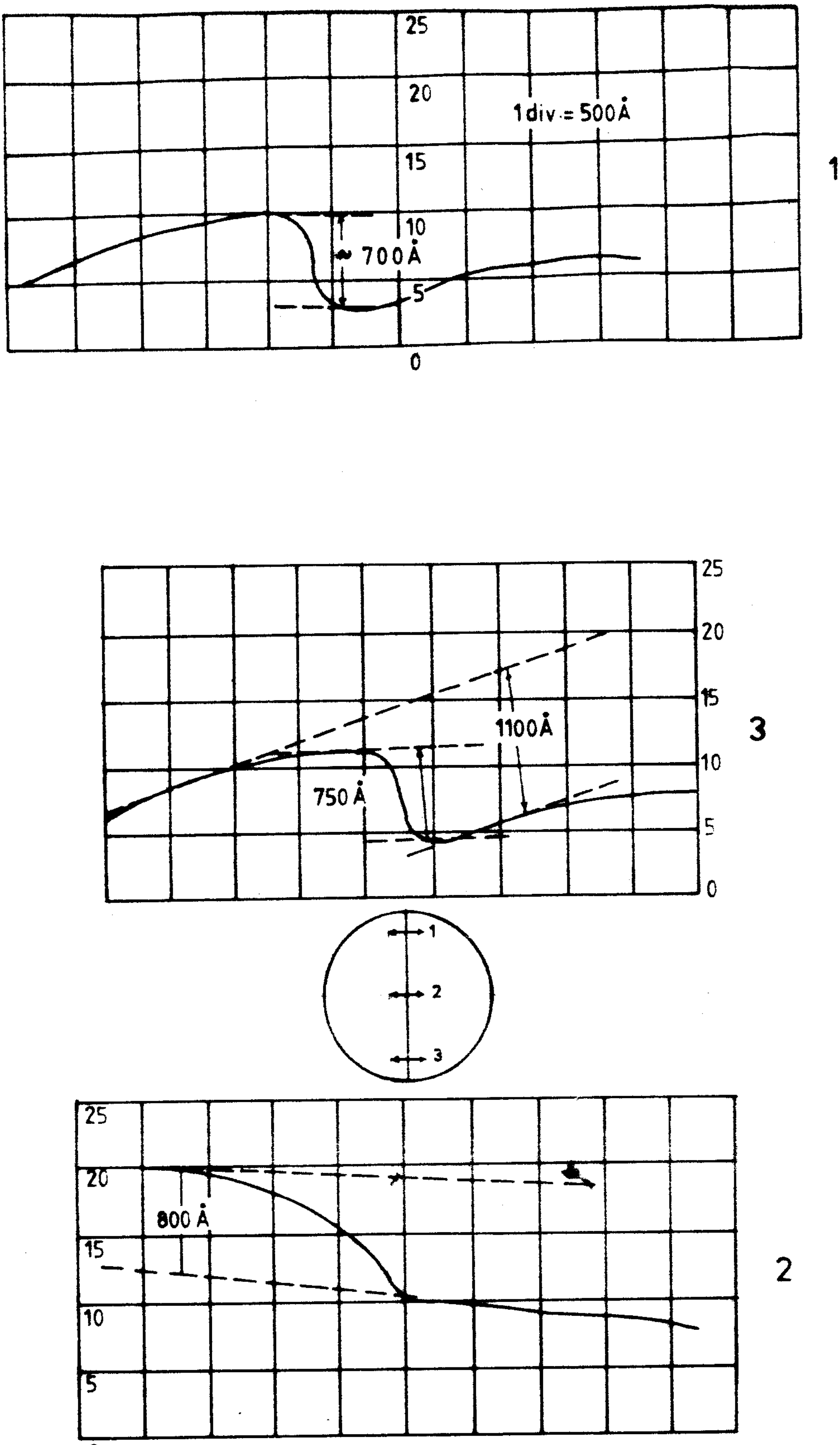

Fig. 21. Thickness of the Cr layer sputtered on to Ga-As at different points of the wafer. A strange profileshape and non-abrupt edge (thickness ≃ 700-800 Å).

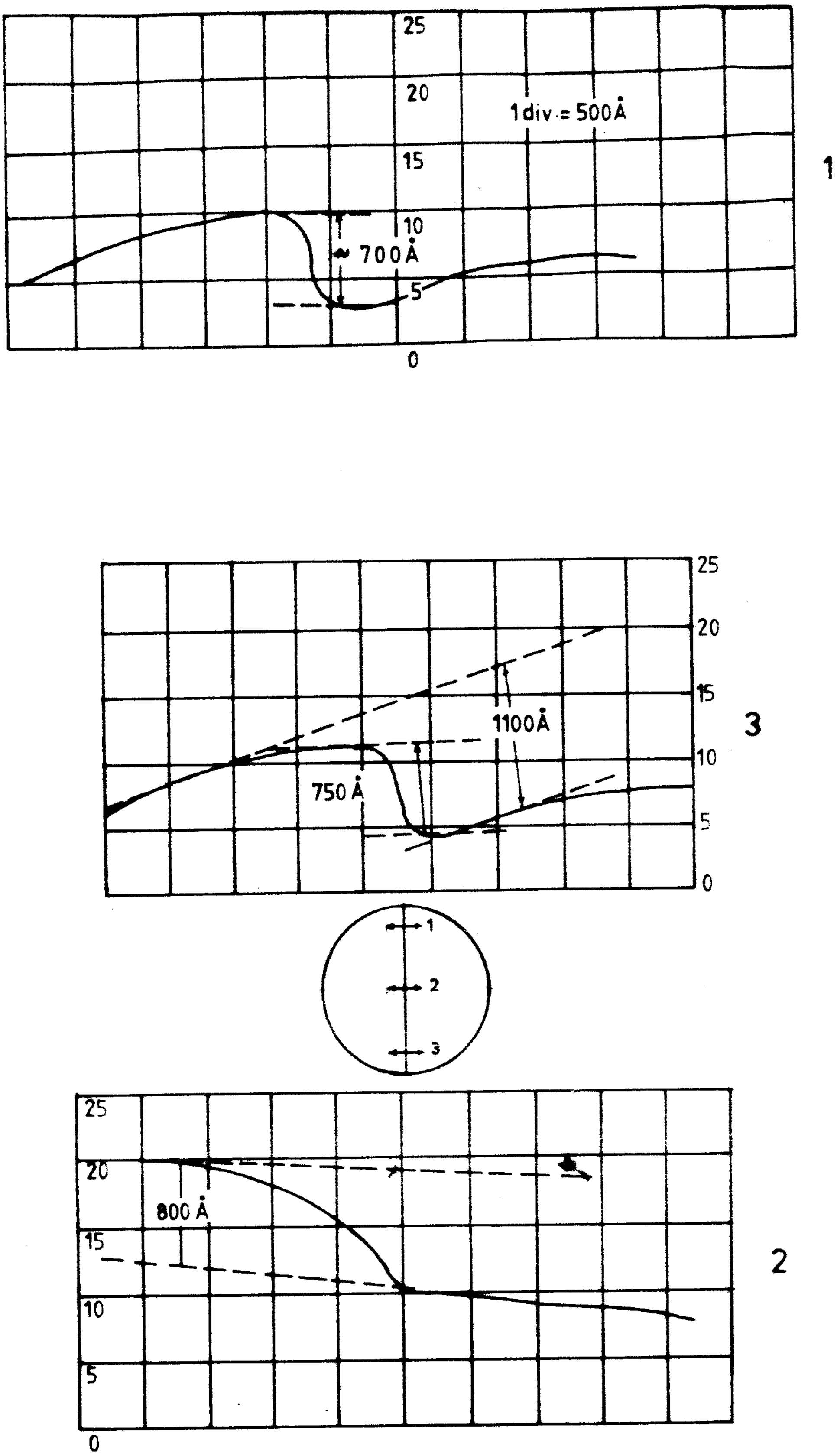

Fig. 21. Thickness of the Cr layer sputtered on to Ga-As at different points of the wafer. A strange profileshape and non-abrupt edge (thickness ≈ 700-800 Å).

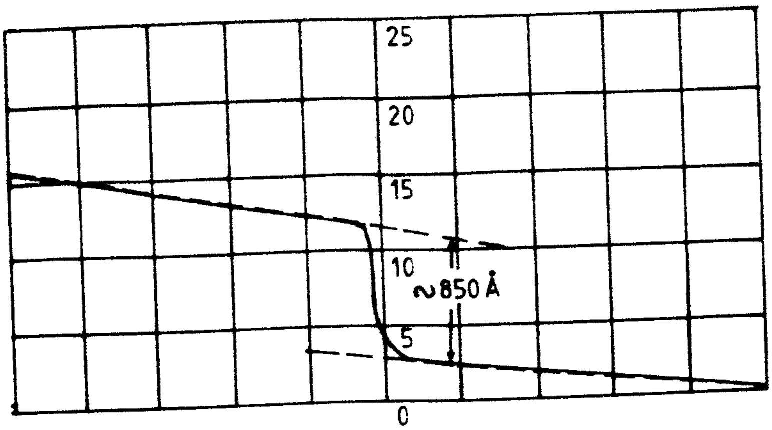

1

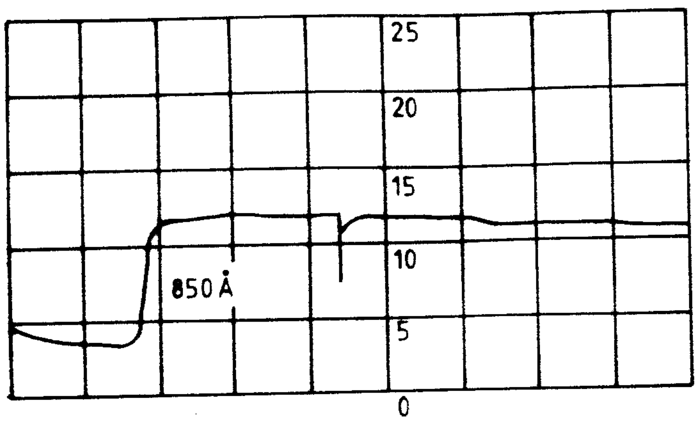

2

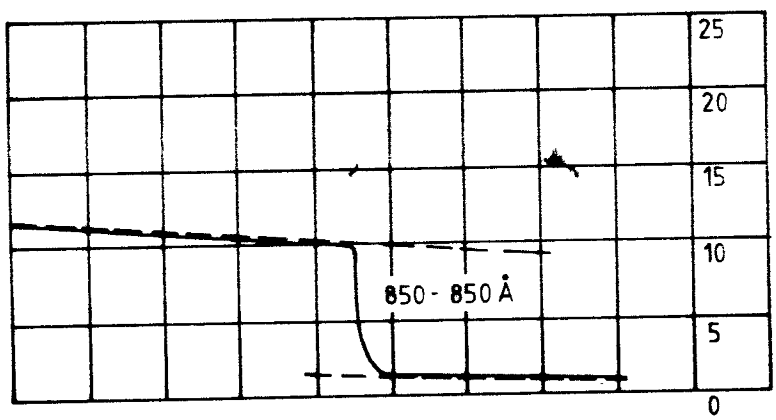

3

Fig. 22. Thickness of the Cr layer sputtered on the Silicon wafer. Somehow, a more uniform profile than Ga A

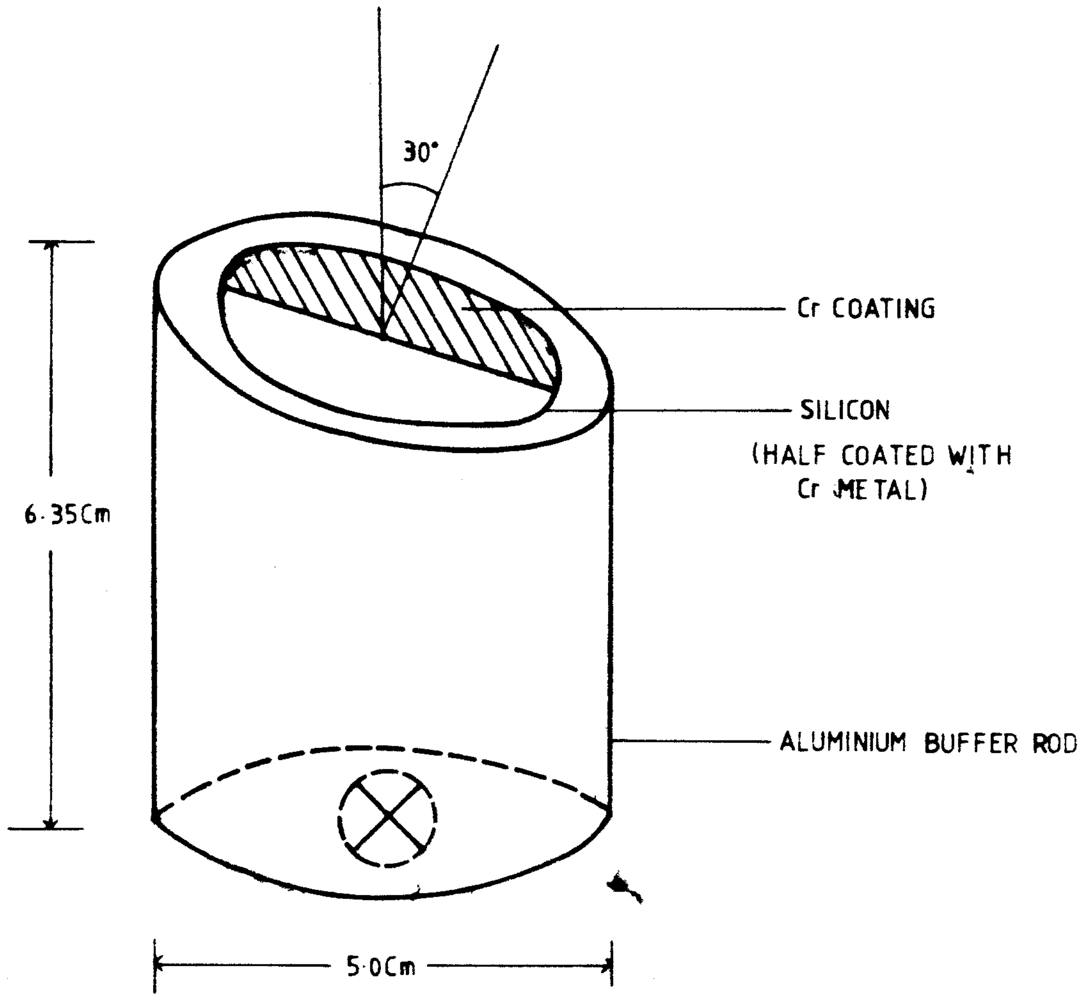

Fig. 23. The configuration of the sample and transducer.

the sensitivity of the later to heat waves. Though the signal is somehow attenuated by the aluminium as it passes through the magnitude of this attenuation is very negligible (about 0.0034dB/mm). From the figure, we can also notice that the semiconductor surface will be at an angle of 30^{o} with respect to the pzt. This has been found to enhance the detection of the generated longitudinal waves, which has been known to show strong directivity with very weak generation at normal incidence of the beam to the absorbing surface[19,20].

3.3. EXPERIMENTAL PROCEDURE

An argon_ion gas laser beam (λ=514.5nm) of a variable beam power, up to 2W (though the operating power used was around 200mW) was used as a light source. The light was passed through an acousto_optic modulator which intensity modulated the beam of light at rates up to 40MHz or greater. Drive power to this acousto_optic modulator was derived from the Intra Action Model ME-40 signal processor. This signal processor, when used with the acousto_optic modulator could be used to amplitude modulate or to shift the optical

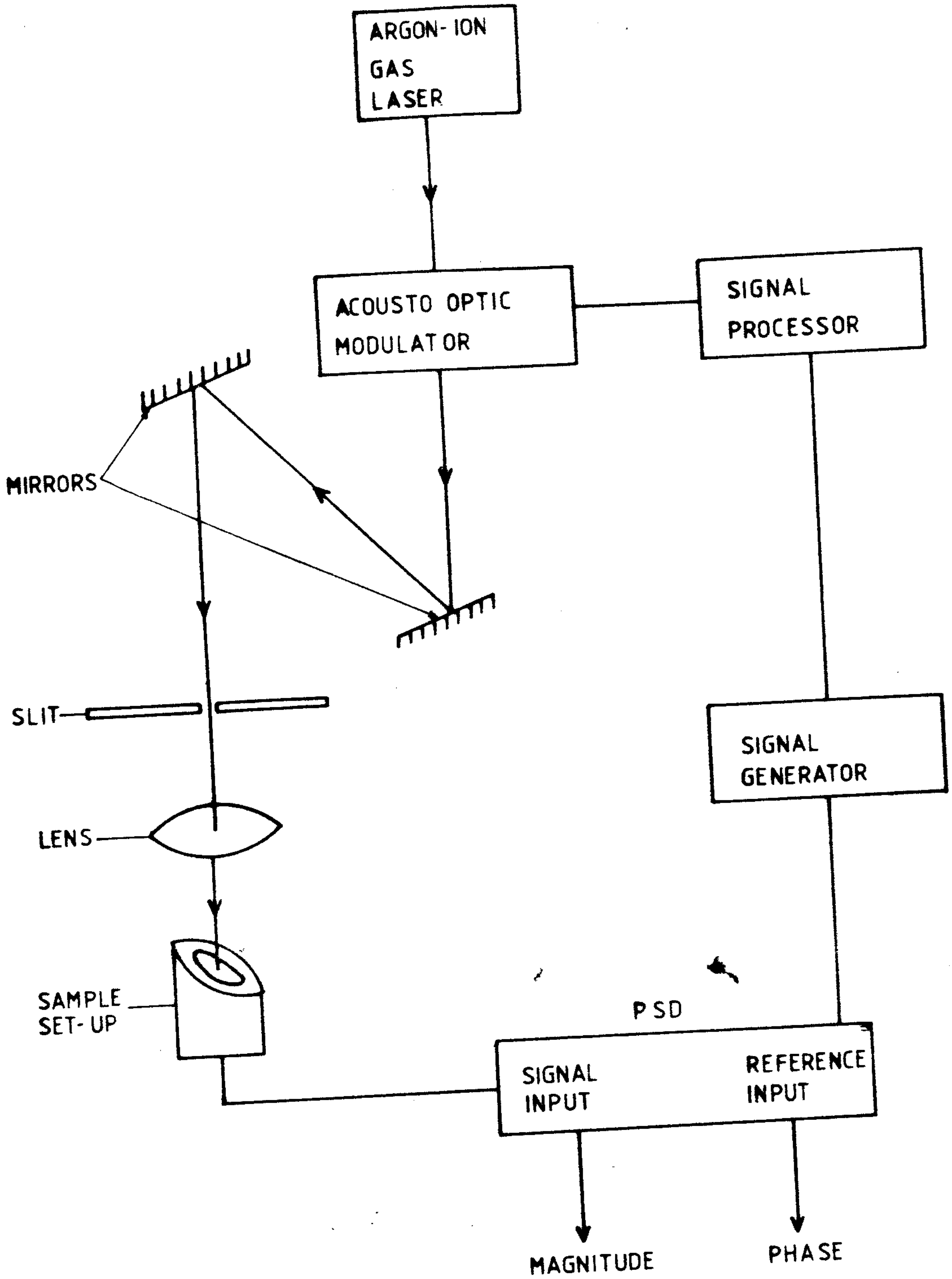

Fig. 24. Schematic of the photoacoustic measurement (Modulation frequency was 200KHz).

frequency of the laser light. In this experiment, it was used to amplitude modulate, from dc to video frequencies, according to the required level. The Model ME-40 accepted an analog input signal and provided a 100 percent amplitude modulated output. An input signal voltage of approximately 1Volt could produce an RF output of 2Watts.

The light beam entering the acousto_optic modulator at nearly normal incidence comes out as a split beam, the deflected and undeflected beams. The angle between the deflected and undeflected beam is dependent upon the light wavelength and the acoustic frequency, $\alpha = 0.26 \times \lambda \times f$. The total deflection angle of 3.25milliradians is proportional to the total frequency deviation, Δf=20MHz, the angle being limited by the piezoelectric transducers which act electrically as a band pass filter. The intensity of the deflected light is proportional to acoustic power. Since the two split beams are still very close to one another and only one beam is needed for the illumination, from the modulator the beams are reflected back and forth by two mirrors in a bid to separate them further apart and isolate one.

After the deflected beam was isolated by allowing it through a small slit and the other blocked, it was focussed by a lens into a spot size of about 120 μm onto the samples.

One after another, each sample was then set up as explained in the previous section. The sample and transducer housing was grounded to prevent charge pick_up signals. The beam was then scanned across the sample surface, from the coated side to the bare semiconductor, or vice versa. At first, the beam was scanned across the entire face, along the diameter of the wafer. However, it turned out during the course of the experiment that there was no reason to do this as it only resulted in variations in the output signal due to the diferences in the sample and coating thicknesses over large scanning distances. So the beam was just confined in a small region, on both sides of the junction to limit it to a uniform thickness. Scanning was accomplished by turning a knob of a vernier scanning mechanism which was holding the sample set up (and incorporating a potentiometer). By turning this knob, the absorbing surface could be moved across the beam. The surface could also be inclined in different positions by a suitable arrangement of knobs making sure that the surface could be placed at different angles to the beam - as the angle of the beam to the sample surface is also very important in generating acoustic signals (Chapter Four)[20]. The response of the samples to the illumination is manifested by the output voltage generated at the pzt transducer, which was directed through the AC Precision Amplifier, Ortec Brookdeal Model 9452. From the amplifier, the signal is then passed through the phase sensitive detection system, an EG&G Princeton Applied Research Two_Phase Lock_in_Analyser, Model 5208, for processing. Both the magnitude and phase of the acoustic signal were measured. The output from the PSD was monitored by an oscilloscope and measured by a digital voltmeter. This output was also combined with the outputs from the potentiometer in the scanning device in such a way as to provide a two_dimensional projection of the signal on the X-Y recorder, with the Y_axis from the output of the PSD giving either the photoacoustic signal magnitude or its phase.

Starting with GaAs, the beam was scanned through the sample absorbing surface and as the beam crosses from the coated (uncoated) side to the uncoated (coated) side, the changes in the magnitude and phase of the signals were observed and recorded on the X-Y recorder, as will be shown in the next chapter, although for silicon there was no response at all for reasons explained later.

CHAPTER FOUR

RESULTS

4.1. VERIFICATION OF THE PHASE RELATIONSHIPS BETWEEN THE ELECTRONIC AND THERMAL PHOTOACOUSTIC SIGNALS

Starting with GaAs, Figures 25-27 show the magnitude and the phase of the generated acoustic signal relative to the modulated incident laser beam plotted as a function of the position of the beam on the sample. In the bare GaAs, we have the generation of holes and electrons (section 3.3) which results in the so called electronic strain. In the Cr layer, the acoustic generation must only be due to thermal stresses, since essentially no light will penetrate through this layer into the semiconductor and hence there will be no carrier injection. Clearly, neither the behaviour of the magnitude nor the phase are in good agreement with our theoretical prediction, that the signals due to electronic strain and thermal strain should be in phase. The measurements were repeated on three different points (see Fig.21.) of the sample

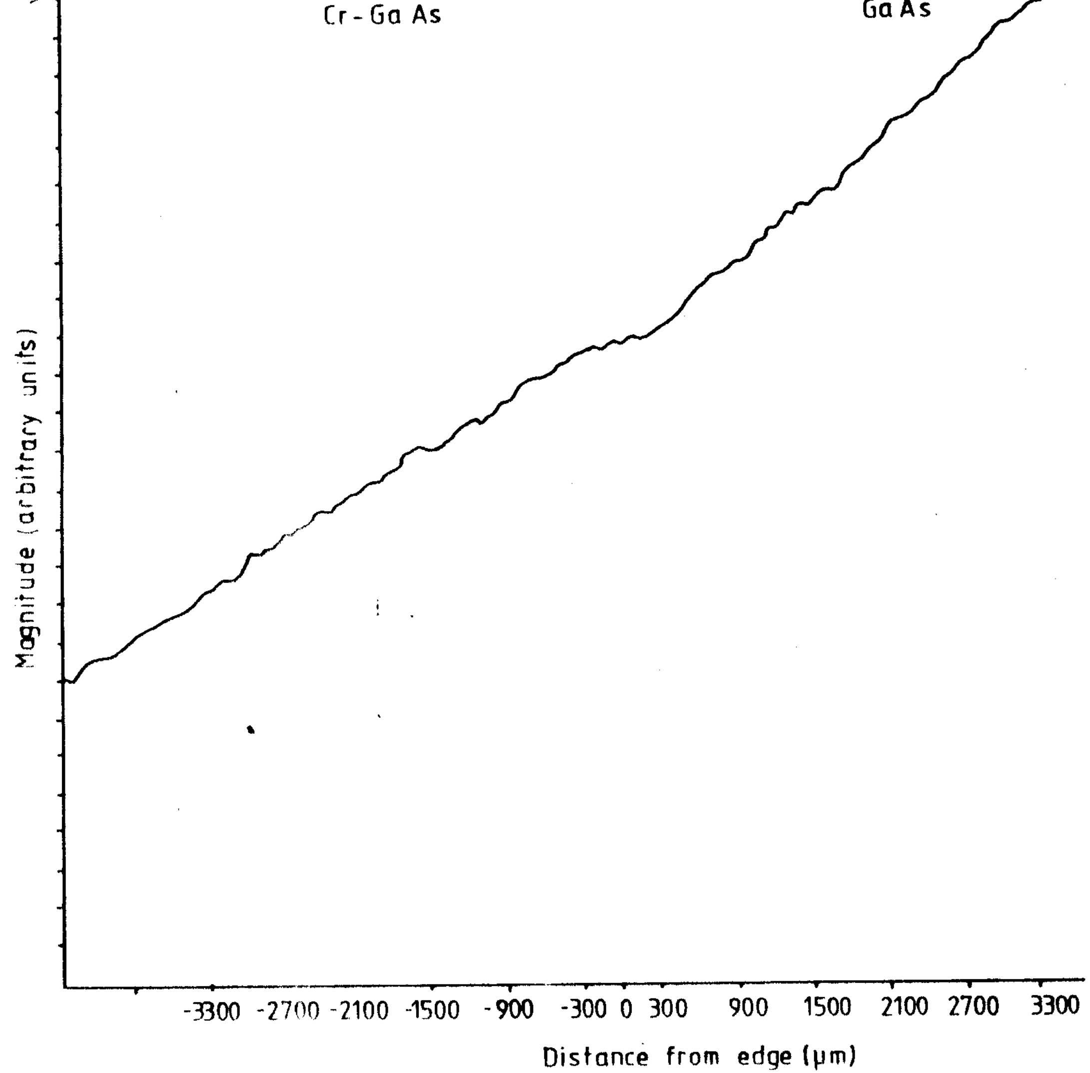

Fig.25(a). Magnitude of the Transducer Output (negative values refer to the region of metallized GaAs and positive values to the region of unmetallized GaAs).

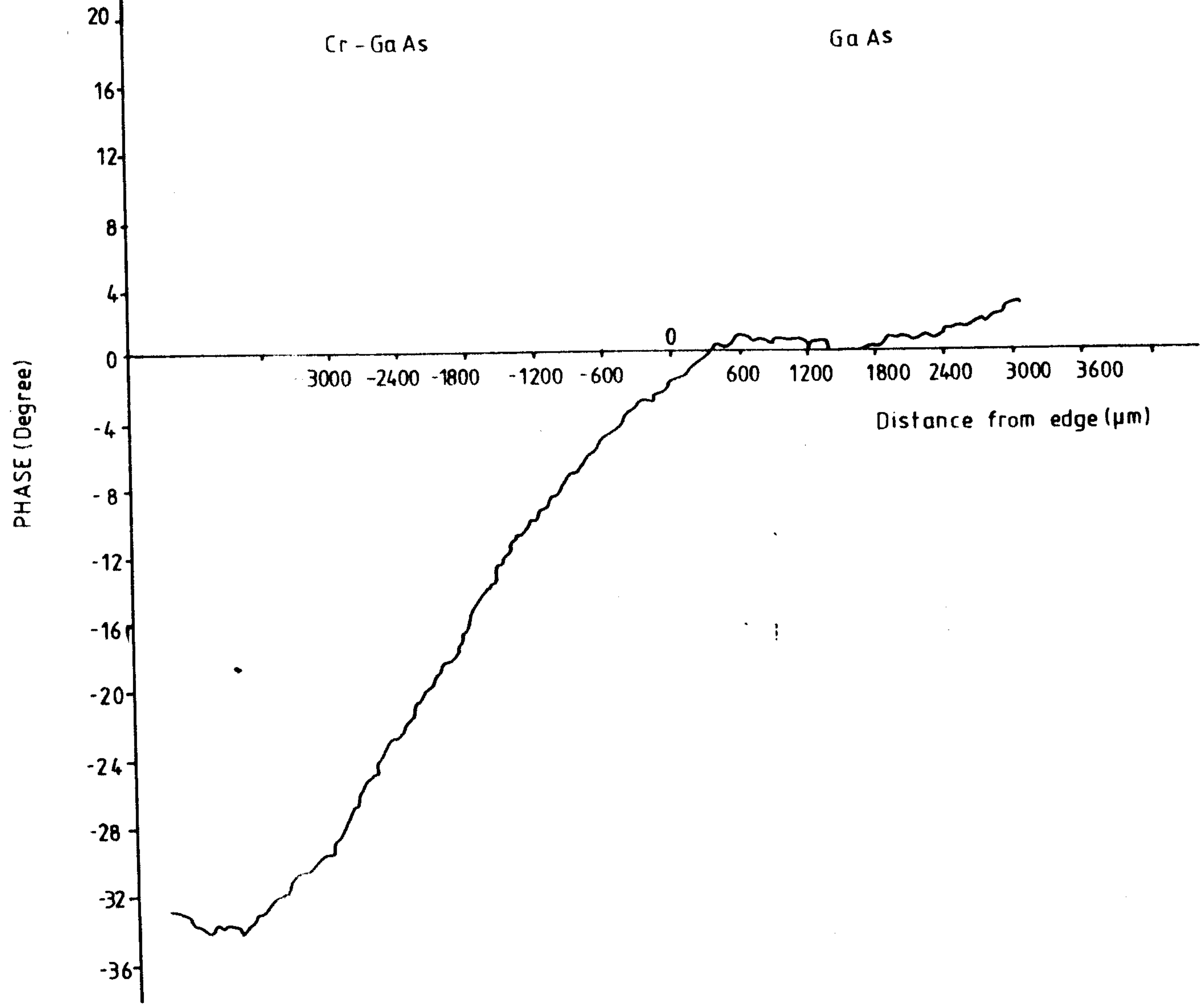

Fig.25(b). Phase of the output relative to the modulation of the laser beam versus the position of the beam spot on the sample.

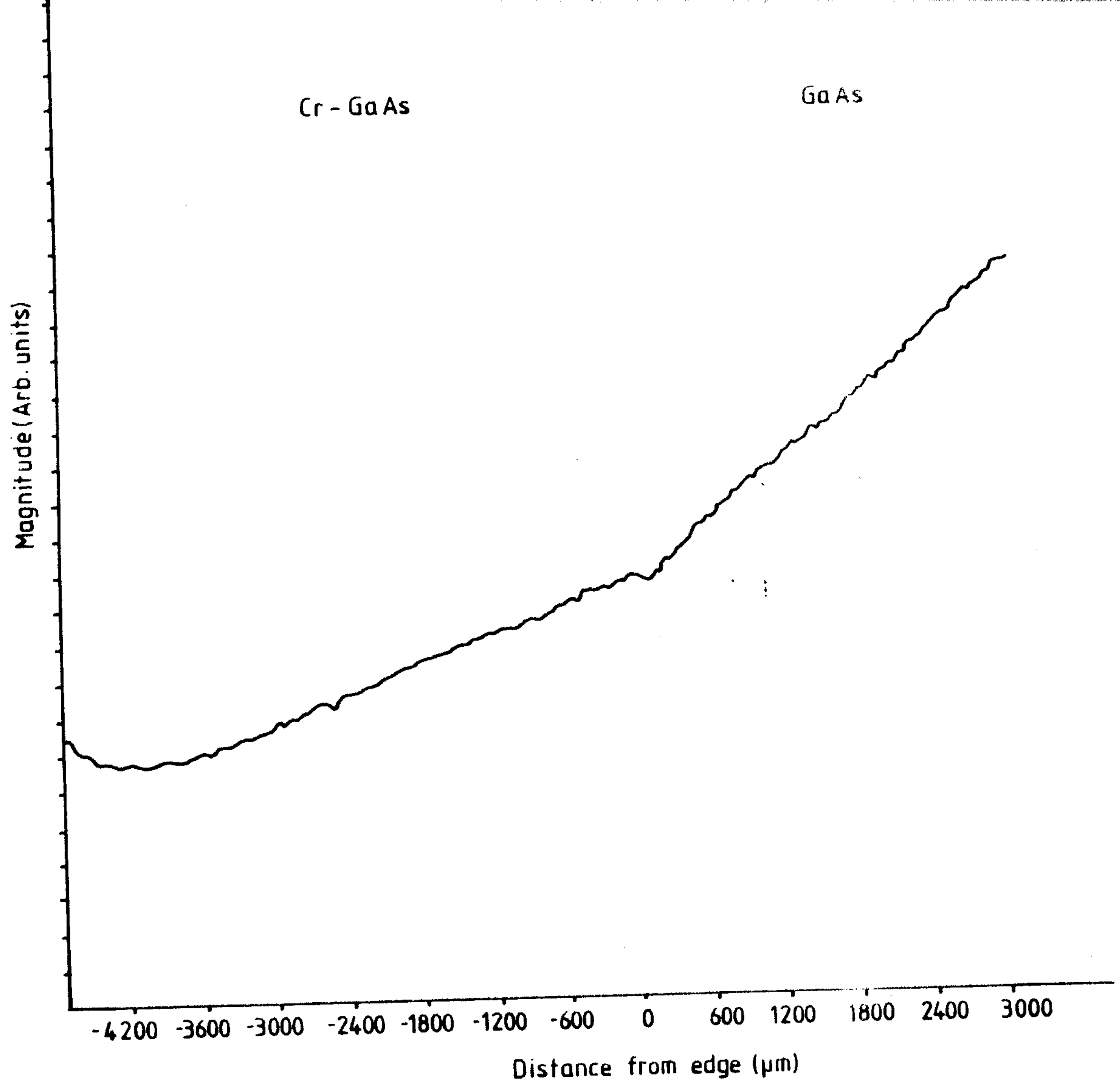

Fig.26(a). Transducer output magnitude as the beam is scanned through the junction.

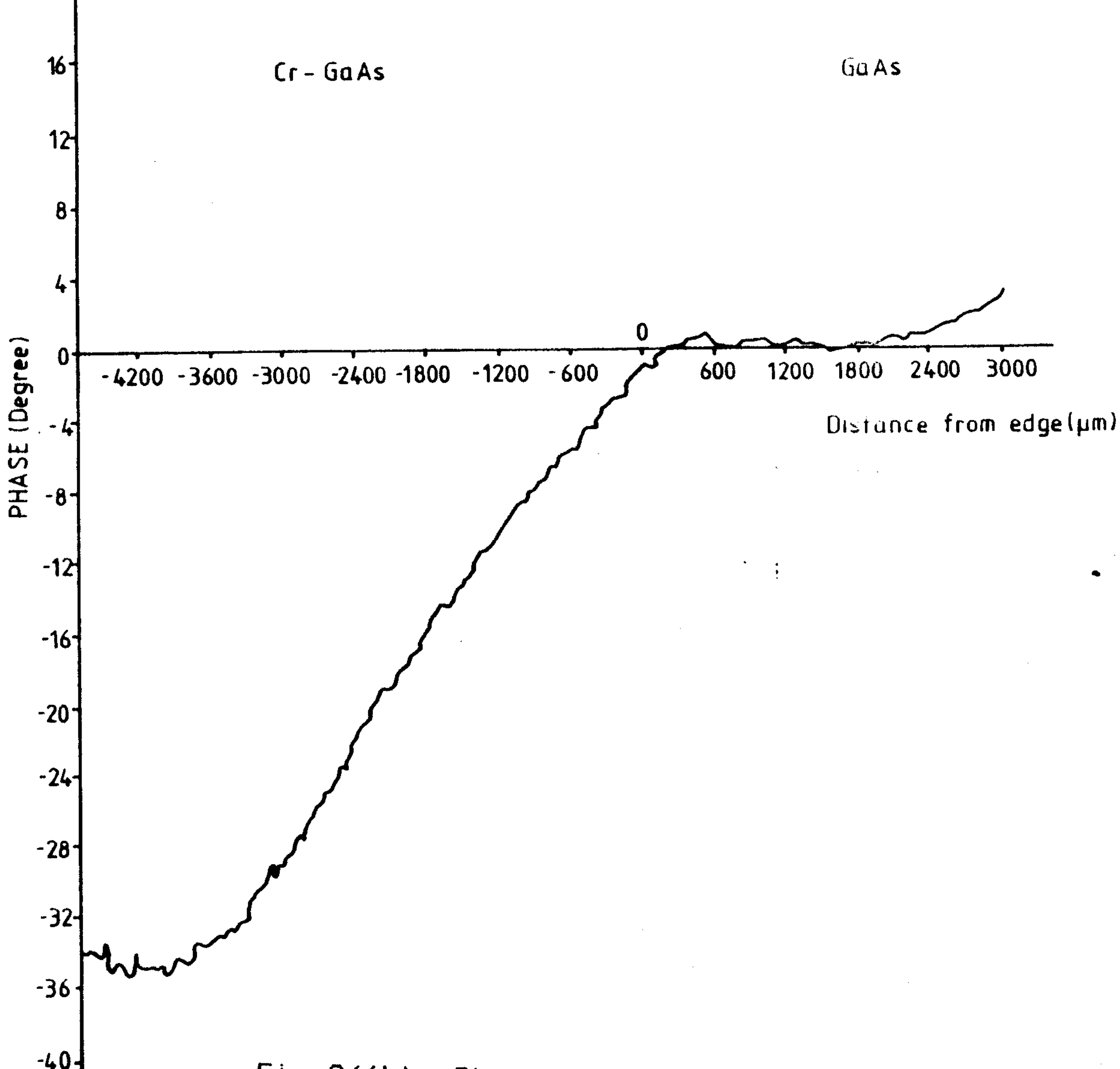

Fig.26(b). Phase of output relative to the modulation plotted against the position of the beam on the sample.

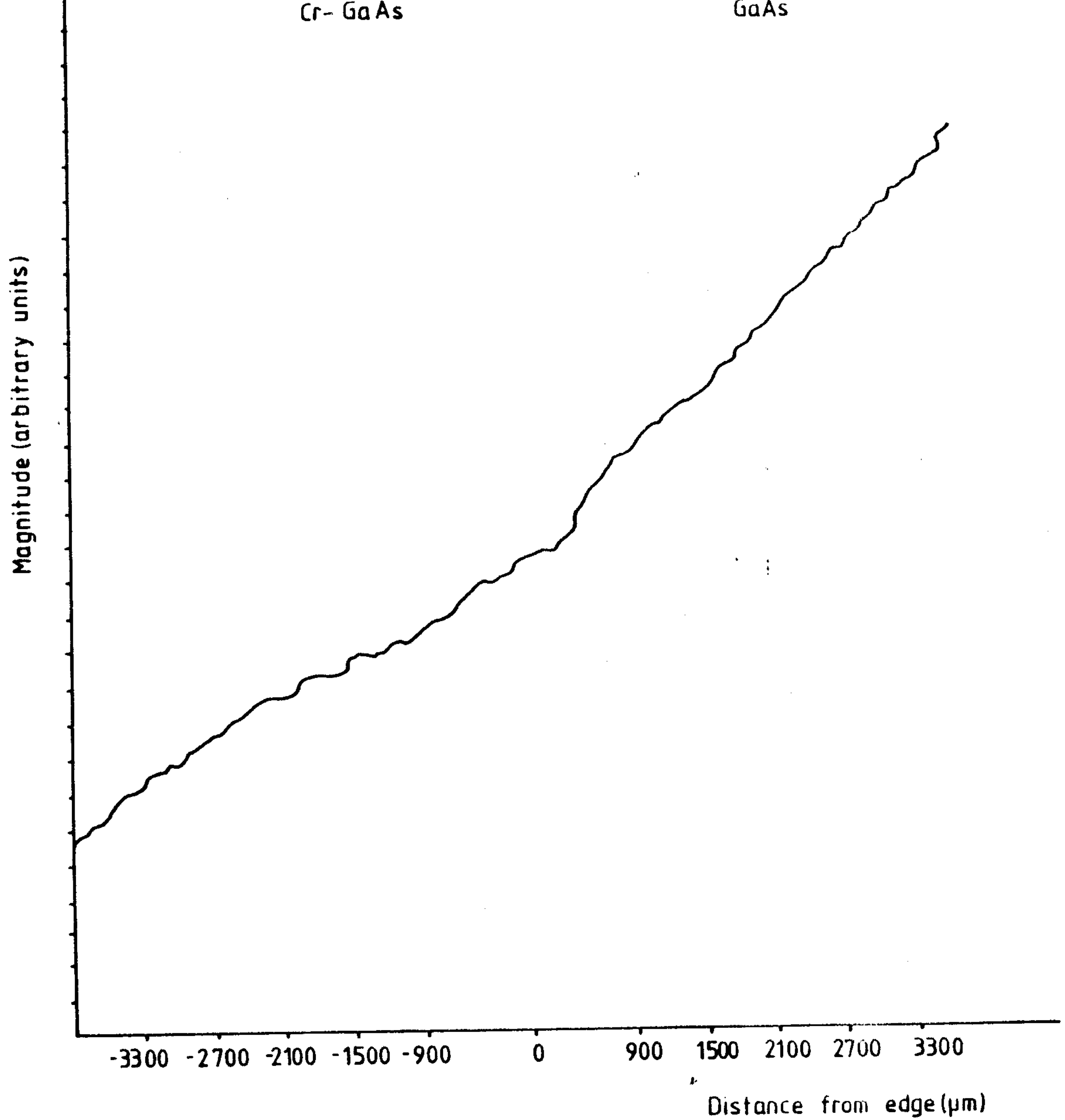

Fig.27(a). Output magnitude plotted against the beam position on sample surface.

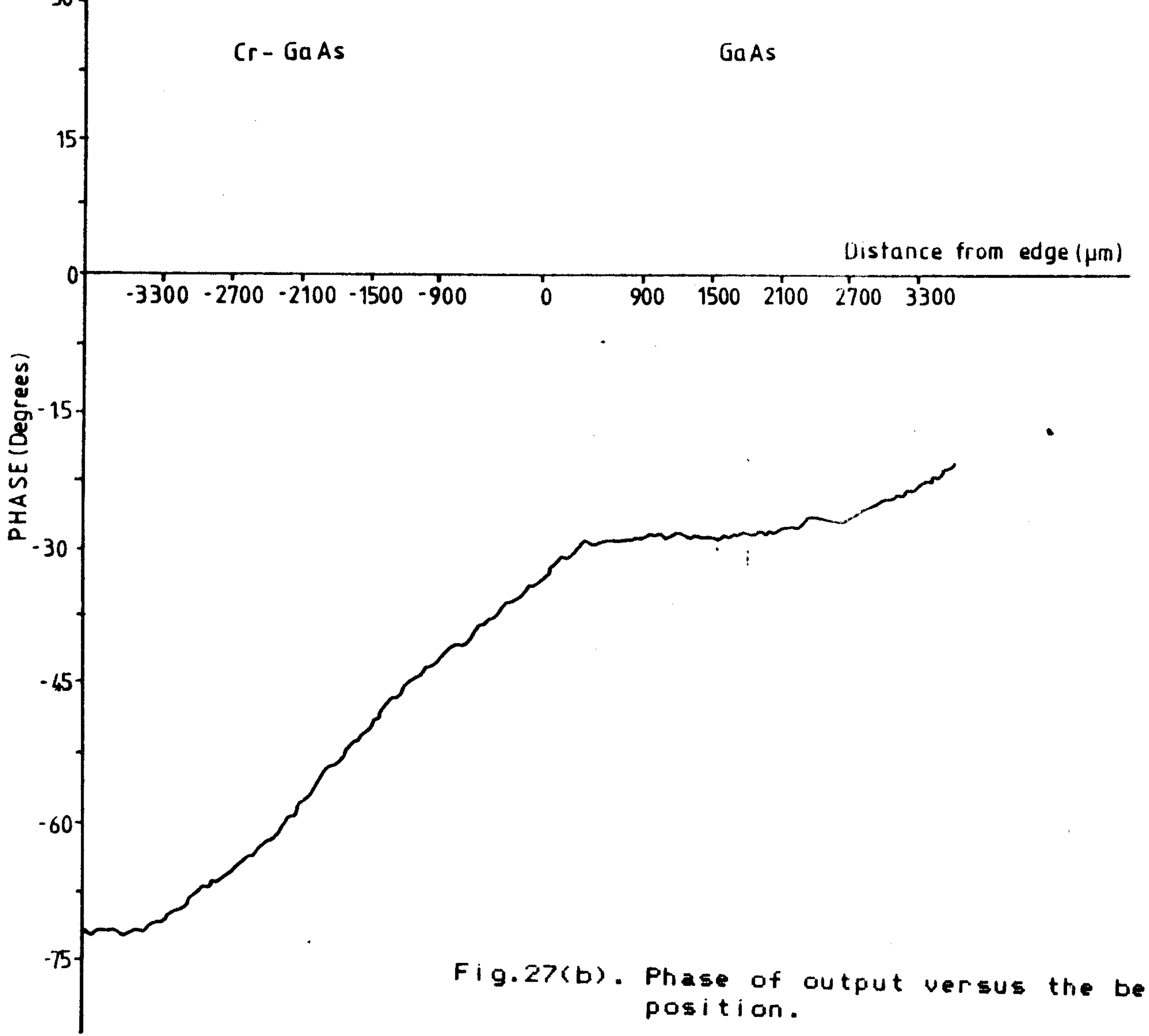

Fig.27(b). Phase of output versus the beam position.

surface in order to confirm this change in phase and in each case, almost the same kind of behaviour was obtained. They all showed a change in phase of between $30^{o}-40^{o}$ as the beam moves from the bare GaAs to the metallized side. In the case of the magnitude, there is also a continous drop in the same direction of scanning. The drop is such that it appears to be almost linear and the position of the junction is not well defined on the curves. The change in magnitude of the acoustic signal as the beam reaches the edge of metallization is not well shown on the results, so that it becomes somewhat difficult to explain this kind of behaviour.

As for silicon there was no acoustic signal detected on both sides of the junction. It was a pity that despite repeated attempts using a very powerful laser beam (500mW), it was not possible to obtain any acoustic waves in the sample that could be detected by the transducer. The whole range, 1Hz-1MHz, of frequency was tried but throughout, there was nothing at the output except noise. It was later discovered that we needed to modulate the beam of light at very high frequencies (in the MHz range) in order to register some acoustic signals. Unfortunately, the limitation of the operating frequency range (only up to 500KHz) of the measuring system (the PSD) could not permit measurements to be done at such high frequencies. It was assumed that the carrier lifetime in silicon must have been much less than that of GaAs, so that the rate of recombination of carriers is much higher than the generation rate at these low modulation frequencies, hence there is an absence of strain during the pulse duration. So we needed modulation frequencies so high that the rate at which carriers are produced is much higher than the rate at which they recombine in order to maintain a steady state strain situation which could then be easily detected by the transducer.

It is therefore useful to include the experimental results given by Stearns and Kino[20] in order to demonstrate clearly what had been expected. Fig.28. shows the results they obtained on their silicon sample. As the beam crosses from one side of the junction to the other, there is a 180^{o} phase shift occuring in the signal. In addition to the difference in sign of the two strains, as discussed in section 1.3., the results

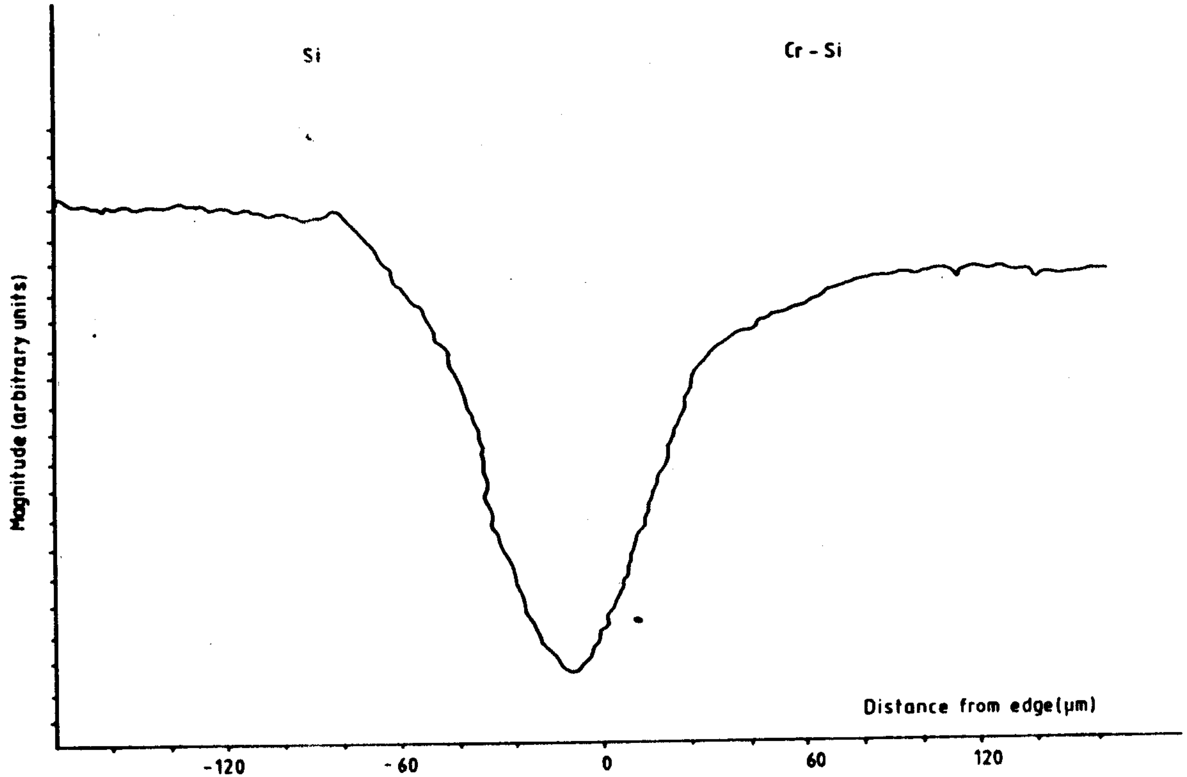

Fig.28(a). Magnitude of the Photoacoustic signal as the laser beam is scanned across the edge of Cr metallization. (Stearns & Kino)

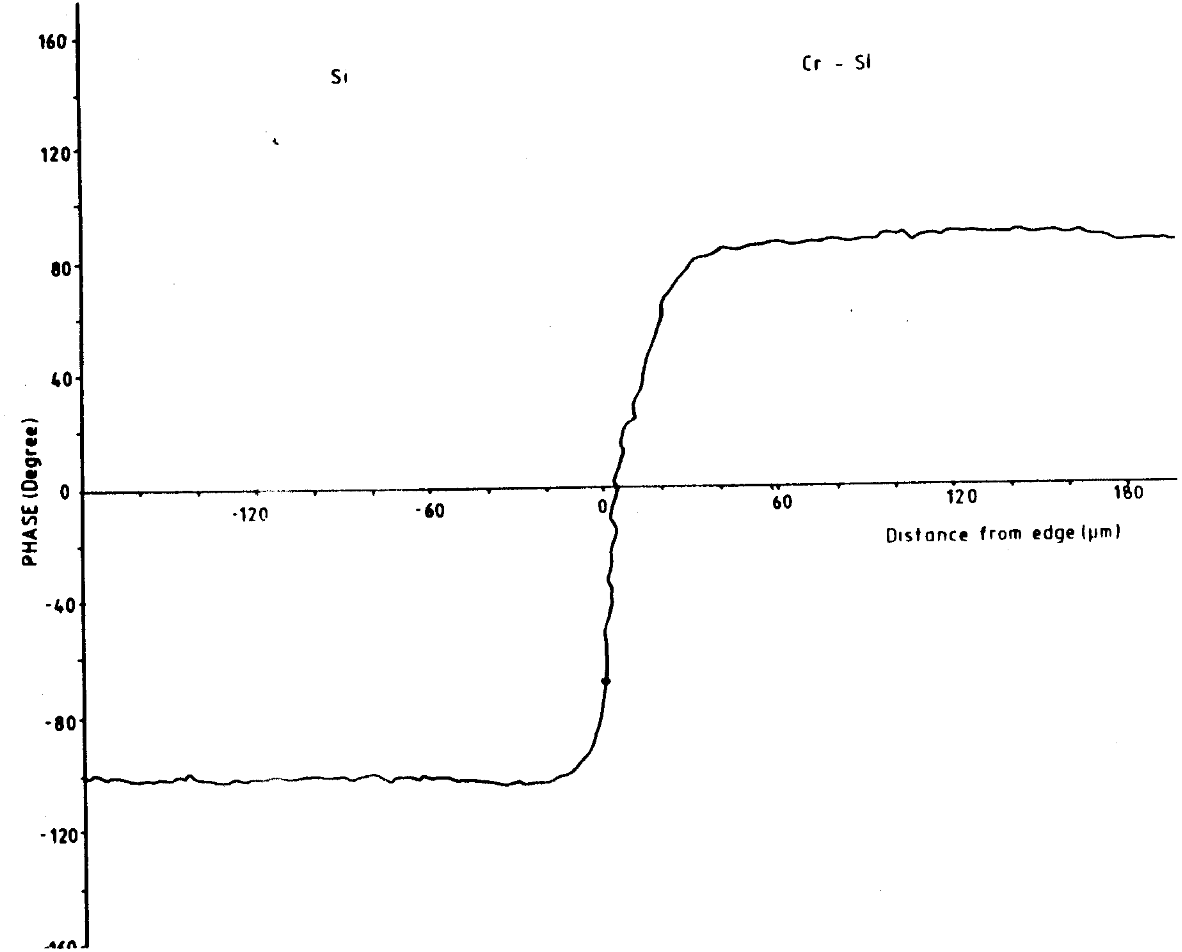

Fig.28(b). Phase of the output relative to the modulation frequency of the incident laser beam plotted as a function of the beam position on the sample surface (Stewart&King)

also seem to suggest that the electronic strain is the dominant contributor to the generated acoustic waves in the uncoated side of the silicon. It can be noted that Stearns and Kino used a very tiny spot size ($\simeq$20μm) and scanned through a very small distance, $\simeq$120μm on both sides of the boundary. We expected to produce similar results though we were scanning through a larger distance, but what was obtained were very unsatisfactory and inconclusive results. What was being detected was all noise in the system.

Going back to GaAs, the phase shift we expected in the acoustic signal was not clearly obtained as the phase kept changing with the scanning distance, on both sides of the sample. In addition to the problem of the big spot size, which obscured the fine detail that is revealed in experiments where very tiny spot sizes are used (for a example in Stearns & Kino's case), there was also the effect of the strange profile of the thickness of the Cr layer resulting into a non_abrupt edge (Fig.21.), which is manifested in the results. As for the spot size, it was so big (120μm) that when it is at the boundary, it actually illuminated both sides of the junction so that there is no good resolution of the GaAs_Cr.GaAs junction. As a result, it was difficult to observe any abrupt change as the beam crossed the junction.

4.2. CALCULATION OF THE ELECTRONIC AND THERMAL PHOTOACOUSTIC SIGNALS

In this work, hf=2.42eV, and for GaAs, dE_g/dp = 1.72×10^{-24} cm^{-3} , E_g =1.47eV, α =5.73×10^{-6} $^{o}K^{-1}$, ρ=5320 Kgm^{-3} and c =418.68 JKg^{-1} $^{o}C^{-1}$. Substituting these into the bracketed expression in equation (1.32) we find that the contribution of the electronic strain to the total photoacoustic signal is approximately 10 times, that of the thermal strain, compared to the -2.6 times in silicon calculated by Stearns and Kino. This indicates that the electronic strain contribution is larger in direct band_gap GaAs than in the indirect band_gap silicon.

The ratio of the transducer response when the laser beam is incident on the semiconductor to the response when incident on the metallized side is the ratio of equations (1.32) and (1.33). Substituting in the values , and in the experiment R_{GaAs}=0.33 and R_{Cr}=0.25, we obtain $(V_{GaAs}/V_{Cr}) \simeq 4.65$.

A comparison of these calculations with the magnitudes of the acoustic signal found on both sides of the sample in the results in Figures 25-27 (for GaAs), we only see a good agreement at the extreme ends of the curve. But even so, there does not seem to be any consistency in this ratio in the rest of the region, due to the changing of the signal. Stearns and Kino calculated for their silicon and they found -1.3. In both cases, we see that the electronic effect is still the dominant contributor, to the acoustic signal.

CHAPTER FIVE

DISCUSSION AND CONCLUSION

5.1. DISCUSSION

This experiment was set to investigate the effect of both electronic and thermal strains in both the direct band_gap semiconductor (GaAs) and the indirect band_gap semiconductor (silicon). It was also to prove that the two strains are of the same sign in direct band_gap semiconductors and of different signs in the case of indirect band_gap semiconductors by verifying whether the two signals are in phase or 180^{o} out of phase with one another. From the results in the last chapter, there seems to have been a successful attempt in GaAs. The no_phase shift we anticipated in this sample did not come out clearly because of the 30^{o} -40^{o} phase shift observed. It is quite difficult to explain these results, except to point out that this kind of behaviour appears to have been influenced by some experimental factors, which if they had been corrected, the results may have agreed very well with the theory.

Some of the factors which had a serious bearing on the experimental results are; the thickness of the Cr coating, the beam spot size, and the limit in the modulation frequency imposed by the measuring system.

The thickness of the metallic coating, as we have already seen, was not uniform. The coating decreases as one moves further away from the bare GaAs. This presumably resulted in a corresponding change in the absorption of the light by the surface as the beam is scanned across, resulting in a non_uniform heating of the sample. We needed a very uniform sputtering to avoid any mismatch in the absorption of light

The beam spot size was not ideal for better resolution of the image. We needed a spot size of a few microns in order to obtain a clear and detailed picture of the changes in the signal as the beam crosses the junction. With my beam size of about 120μm, it was found in the course of the experiment that the fine detail which could have been revealed with a tiny spot size was being obscured by the big spot size. Lack of the sophisticated instruments to bring down the spot size to the required level prevented the use of such a spot size.

The other serious setback was in the modulation of the beam. Very high modulation frequencies (in the MHz range) were required, especially for silicon. The fact that the measuring electronics could not operate with signals of frequency over 500KHz meant that we could not modulate the beam at the frequency needed. This limitation deprived the experiment of a very important parameter, that of working at 1MHz and above. That is why in silicon no signals were being detected at the frequencies used because carriers recombined quicker than they are generated and hence there was no strain registered within the period of illumination. The situation would have been better if a PSD system with a very high operating frequency was used, for then modulation frequencies of over 500KHz would have been possible to use.

5.2. CONCLUSION

The lack of success in the experimental work is a pity but the work has revealed several important points to which greater attention will have to be paid, if I continued the work. In addition to the few points already raised in the above section, we need to mention the bond between the semiconductor and the aluminium buffer rod. This bond could affect the value of Δ° but as long as the bond is uniform over the scanned distance, the calculations done are independent of Δ° and thus unaffected by the bond. I think more care is needed to identify the crystallographic orientation of the samples and their mounting.

It should also be mentioned that the experiment suffered from acoustic wave resonance in the aluminium and this would account for why we got almost no response in certain positions of the spot. It would be worthwhile to test this resonance by setting up the system with a number of pzt transducer chips on the faces and look at the response from one driven chip to the others used as detectors.

Photoacoustic Spectroscopy, however, appears to hold considerable promise as both a general analytical tool and as a dedicated process_control instrument for the semiconductor industry, especially in sensors and alarms. Photoacoustic methods can be employed in a semiconductor fabrication line to monitor the presence of electrical shorts or leaks in integrated circuits at a very early stage of the device fabrication.

Photoacoustics may also be used to visualise and inspect patterns and structures that are below the surface and to perform localized thin film thickness measurements. With these various capabilities photoacoustics seems to be heading for major applications in large_scale integrated circuits, sensors and other electronic and semiconductor devices.

REFERENCES

1. R.M.White, J. Appl. Phys. 34, 3559 (1963).

2. M.J.Brienza and A.J.DeMaria, Appl. Phys. Lett. 11, 44 (1967).

3. K. Kubota, Solid State Commun. 9, 2045 (1971).

4. L.B.Kreuzer and C.K.N.Patel, Science 173, 45 (1971).

5. A.G.Bell, Am. J. Sci. 20, 305 (1880).

6. Y.H.Wong, R.L.Thomas, and G.F.Hawkins, Appl. Phys. Lett. 32, 538 (1978).

7. R.L.Thomas, J.J.Pouch, Y.H.Wong, L.D.Fauro, P.K.Kuo, and A.Rosencwaig, J. Appl. Phys. 51, 1152 (1980).

8. A.Rosencwaig and G.Busse, Appl. Phys. Lett. 36, 725 (1980).

9. G.Busse and A.Rosencwaig, Appl. Phys. Lett. 36, 815 (1980).

10. E.Brandis and A.Rosencwaig, Appl. Phys. Lett. 37, 98 (1980).

11. A.Rosencwaig, Science 218, 223 (1982).

12. H.K.Wickramasinghe, R.C.Bray, V.Jipson, C.F.Quate, and J.R.Salcedo, Appl. Phys. Lett. 33, 923 (1978).

13. A.Rosencwaig and R.M.White, Appl. Phys. Lett. 38, 165 (1981).

14. T.Figielski, Phys. Status Solidi 1, 306 (1961).

15. C.Kittel, Introduction to Solid State Physics, John Wiley & Sons, Inc., New York (1956), 2nd ed. (p.91).

16. J.F.McClelland and R.N.Kniseley, Appl. Opt. 15, 2658 (1976).

17. A.Rosencwaig, Am. Lab. 11, 39 (1979).

18. H.S.Carslaw and J.C.Jaeger, Conduction of Heat in Solids, Oxford University Press, London (1959), 2nd ed. (p.64).

19. C.B.Scruby, R.J.Dewhurst, D.A.Hutchins, and S.B.Palmer, AERE Harwell Report No. 10099, Oxfordshire, England, Department of Applied Physics, University of Hull (May, 1981).

20. G.S.Kino and R.G.Stearns, Appl. Phys. Lett. 47, 926 (1985).

21. R.G.Stearns and G.S.Kino, Appl. Phys. Lett. 47, 1048 (1985).